BRNO UNIVERSITY OF TECHNOLOGY

VYSOKÉ UČENÍ TECHNICKÉ V BRNĚ

FACULTY OF ELECTRICAL ENGINEERING AND COMMUNICATION

FAKULTA ELEKTROTECHNIKY
A KOMUNIKAČNÍCH TECHNOLOGIÍ

DEPARTMENT OF POWER ELECTRICAL AND ELECTRONIC ENGINEERING

ÚSTAV VÝKONOVÉ ELEKTROTECHNIKY A ELEKTRONIKY

CONTACTLESS LOADING AND MEASUREMENT OF HIGH-SPEED MACHINES

BEZKONTAKTNÍ ZATĚŽOVÁNÍ A MĚŘENÍ VYSOKOOTÁČKOVÝCH STROJŮ

MASTER'S THESIS
DIPLOMOVÁ PRÁCE

AUTHOR — **Bc. Zbyněk Vojče**
AUTOR PRÁCE

SUPERVISOR — **doc. Ing. Ondřej Vítek, Ph.D.**
VEDOUCÍ PRÁCE

BRNO 2018

VYSOKÉ UČENÍ TECHNICKÉ V BRNĚ
FAKULTA ELEKTROTECHNIKY A KOMUNIKAČNÍCH TECHNOLOGIÍ

Diplomová práce

magisterský navazující studijní obor **Silnoproudá elektrotechnika a výkonová elektronika**
Ústav výkonové elektrotechniky a elektroniky

Student: Bc. Zbyněk Vojče ***ID:*** 164437
Ročník: 2 ***Akademický rok:*** 2017/18

NÁZEV TÉMATU:

Bezkontaktní zatěžování a měření vysokootáčkových strojů

POKYNY PRO VYPRACOVÁNÍ:

1. Seznamte se z principem funkce a konstrukčním řešením vířivých brzd pro vysokootáčkové stroje.
2. Sestavte postup výpočtu a proveďte analytický výpočet vlastností zadané vířivé brzdy.
3. Připravte model vířivé brzdy v programu Maxwell, proveďte výpočet a srovnejte výsledky.
4. Analyzujte možnosti měření krouticího momentu nebo mechanického výkonu vysokootáčkových strojů.

DOPORUČENÁ LITERATURA:

[1] HELLER, Bedřich a HAMATA, Václav. Přídavná pole, síly a ztráty v asynchronním stroji. 1. vyd. Praha: Československá akademie věd, 1961, 202 s.

[2] VÍTEK, Ondřej. Vysokootáčkové elektrické motory, Brno: Vysoké učení technické v Brně, Fakulta elektrotechniky a komunikačních technologií, 2016. 114 s. Habilitační práce.

[3] Časopisecké a konferenční články z databáze IEEE Xplore.

Termín zadání: 5.2.2018 ***Termín odevzdání:*** 21.5.2018

Vedoucí práce: doc. Ing. Ondřej Vítek, Ph.D.
Konzultant:

doc. Ing. Ondřej Vítek, Ph.D.
předseda oborové rady

Abstrakt

Práce se zabývá problematikou měření momentu u velmi vysokootáčkových strojů. Z důvodů vysokých rychlostí jsou tradiční metody měření momentu nepoužitelné, z tohoto důvodu je nutno vyvinout novou bezkontaktní metodu. Pro měření je zvolena metoda zatěžování vířivou brzdou, pro kterou je proveden analytický výpočet jejích vlastností pomocí Maxwellových rovnic a je vytvořen model vířivé brzdy v programu FEMM a Ansys/Maxwell 2D. Na závěr jsou výsledky simulací a výpočtů porovnány s měřením na prototypech brzdy.

Klíčová slova

Měřící metoda, elektromagnetická vířivá brzda, simulace, brzdný výkon, model, měření.

Abstract

Work deals with problematic of torque measurement for very high speed machines. Because of high speeds are traditional torque measuring tools unusable, for this reason is needed to develop new contactless measurement method. For measurement is selected Eddy current brake method, for which an analytical calculation of its properties using Maxwell's equations is performed and a model of Eddy current brake in program FEMM and Ansys/Maxwell 2D is created. In the end the results of simulations and calculations are compared with measurements on brake prototypes.

Keywords

Measurement method, Eddy current brake, simulation, braking power, model, measurement.

Bibliografická citace:

VOJČE, Z. Bezkontaktní zatěžování a měření vysokootáčkových strojů. Brno: Vysoké učení technické v Brně, Fakulta elektrotechniky a komunikačních technologií, 2018. 43 s. Vedoucí diplomové práce doc. Ing. Ondřej Vítek, Ph.D..

Prohlášení

„Prohlašuji, že svou závěrečnou práci na téma Bezkontaktní zatěžování a měření vysokootáčkových strojů jsem vypracoval samostatně pod vedením vedoucího diplomové práce a s použitím odborné literatury a dalších informačních zdrojů, které jsou všechny citovány v práci a uvedeny v seznamu literatury na konci práce.
Jako autor uvedené závěrečné práce dále prohlašuji, že v souvislosti s vytvořením této závěrečné práce jsem neporušil autorská práva třetích osob, zejména jsem nezasáhl nedovoleným způsobem do cizích autorských práv osobnostních a jsem si plně vědom následků porušení ustanovení § 11 a následujících autorského zákona č. 121/2000 Sb., včetně možných trestněprávních důsledků vyplývajících z ustanovení části druhé, hlavy VI. díl 4 Trestního zákoníku č. 40/2009 Sb.

V Brně dne 21. Května 2018 ……

podpis autora

Poděkování

Děkuji vedoucímu diplomové práce doc. Ing. Ondřeji Vítkovi, Ph.D. za účinnou metodickou, pedagogickou a odbornou pomoc a další cenné rady při zpracování mé diplomové práce.

V Brně dne 21. Května 2018 ……

podpis autora

Table of contents

1. Introduction 1
2. Measured very high speed pmsm 2
3. Torque Measurement methods for vhs 4
   - 3.1 Two identical machines method 4
   - 3.2 Inertial method 4
   - 3.3 Eddy current brake method 4
   - 3.4 Ball bearing method 4
4. Eddy current brake design and principle 5
   - 4.1 Principle of Eddy current brake 5
   - 4.2 Design and types of Eddy current brake 6
     - 4.2.1 Axial-flux Eddy current brakes 7
     - 4.2.2 Radial-flux Eddy current brakes 7
5. Analytical Calculation 8
   - 5.1 Eddy current loss 8
6. FEM model of Eddy current brake in femm and Ansys maxwell 15
   - 6.1 Finite element method magnetic 16
   - 6.2 FEM in Ansys Maxwell 18
7. Measurement 22
8. Results comparision 24
   - 8.1 Results for 50 krpm 24
   - 8.2 Results for 100 krpm 26
   - 8.3 Results for 150 krpm 28
   - 8.4 Results for 200 krpm 29

Conclusion 31

List of figures

Fig 2.1 Slotless stator with a sleeve retaining the PM [2] 2
Fig 2.2 Example of slotless litz wire winding 3
Fig 2.3 Measured motor design 3
Fig 4.1 Configuration of axial-flux Eddy current brake [7] 7
Fig 4.2 Configuration of radial-flux Eddy current brake [7] 7
Fig 6.1 Table of prototype ECB dimensions and properties 15
Fig 6.2 Design of ECB with periodic boundary conditions and winding simulating PM 16
Fig 6.3 Detail of winding for PM flux simulation 17
Fig 6.4 Flux density in airgap of ECB at 1 Hz 17
Fig 6.5 Distribution of current density in Aluminum ECB, 100 krpm. 17
Fig 6.6 Design of 3D FEM model of ECB 18
Fig 6.7 Assigned mesh operations on different parts of 2D model 19
Fig 6.8 The distribution of magnetic flux density in ECB for Al conductor, n = 100 krpm 20
Fig 6.10 The distribution of current density in ECB for Al conductor, n = 100 krpm .. 21
Fig 6.9 The distribution of volume loss density in ECB for Al conductor, n = 100 krpm 21
Fig 7.1 Measurement stand for ECB prototype 22
Fig 7.2 Detail of PM and aluminum ECB 23
Fig 7.3 Example of some ECBs 23
Fig 8.1 Braking power in aluminum ECB versus width of conductor at 50 krpm 25
Fig 8.2 Braking power in copper ECB versus width of conductor at 50 krpm 25
Fig 8.3 Braking power in copper ECB versus width of conductor at 100 krpm 27
Fig 8.4 Braking power in aluminum ECB versus width of conductor at 100 krpm 27
Fig 8.5 Braking power in copper ECB versus width of conductor at 150 krpm 28
Fig 8.6 Braking power in aluminum ECB versus width of conductor at 150 krpm 29
Fig 8.7 Braking power in copper ECB versus width of conductor at 200 krpm 30
Fig 8.8 Braking power in aluminum ECB versus width of conductor at 200 krpm 30

List of tables

Table 8.1 Comparison of measured losses in ECB at speed 50 krpm with simulations in FEMM and Ansys Maxwell 2D and analytical calculation 24
Table 8.2 Comparison of measured losses in ECB at speed 100 krpm with simulations in FEMM and Ansys Maxwell 2D and analytical calculation 26
Table 8.3 Comparison of measured losses in ECB at speed 150 krpm with simulations in FEMM and Ansys Maxwell 2D and analytical calculation 28
Table 8.4 Comparison of measured losses in ECB at speed 200 krpm with simulations in FEMM and Ansys Maxwell 2D and analytical calculation 29

1. INTRODUCTION

Recently, due to a technical advantages and an increasing need for compact size, low weight, high power density and high efficiency, utilization of a very high speed (VHS) motors or generators is getting popular in many industrial applications such as centrifugal compressors, vacuum pumps, flywheel energy storage systems, friction welding units and machine tools that require higher speed drives. The higher the motor speed is, the smaller the electric motor volume is for the same power output.

In this work measured VHS machine will be described and for synchronous machine with 200 000 rpm, 670 W, where traditional contact measurement tools are not compatible with such high speeds and low torque, a new contactless torque measurement method will be tested. [3],[4].

2. MEASURED VERY HIGH SPEED PMSM

Measured very high speed (VHS) motor developed by Sobriety s.r.o. is 200 krpm, 670 W PMSM used as a compressor. The machine features a precisely balanced rotor with buried magnet that is mechanically encapsulated to achieve extreme speeds. The rotor is supported by radial and axial bearings of proprietary design that are fully dynamic and operate directly with the machine work fluid. These aerodynamic bearings allow effective operation of the machine at extremely high speeds without any need of secondary lubrication.

According to [2], which compares slotted and slotless stator configurations for VHS, was for its better features selected slotless type of stator (shown in Fig 2.1). Winding is made of litz wires, its disassembled example can be seen in Fig 2.2.

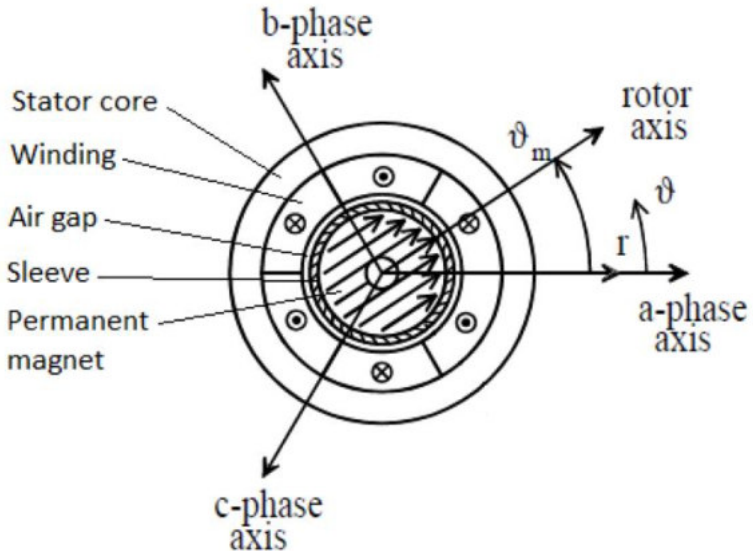

Fig 2.1 Slotless stator with a sleeve retaining the PM [2]

Some of the slotless stator features according to [2] are presented:

a) Slotless motor yields to lower airgap flux density but the current reaction is almost negligible, which means small risk of demagnetization.

b) Stator losses in slotless motor are much lower than in slotted thanks to lower iron losses.

c) When the speed is very high, the slotless solution becomes more advantageous due to rotor losses, since the stator slotting effect disappears and m.m.f. is lower.

d) For slotless version is the ratio D/De higher.

Fig 2.2 Example of slotless litz wire winding

In Fig 2.3 is shown a design of measured compressor.

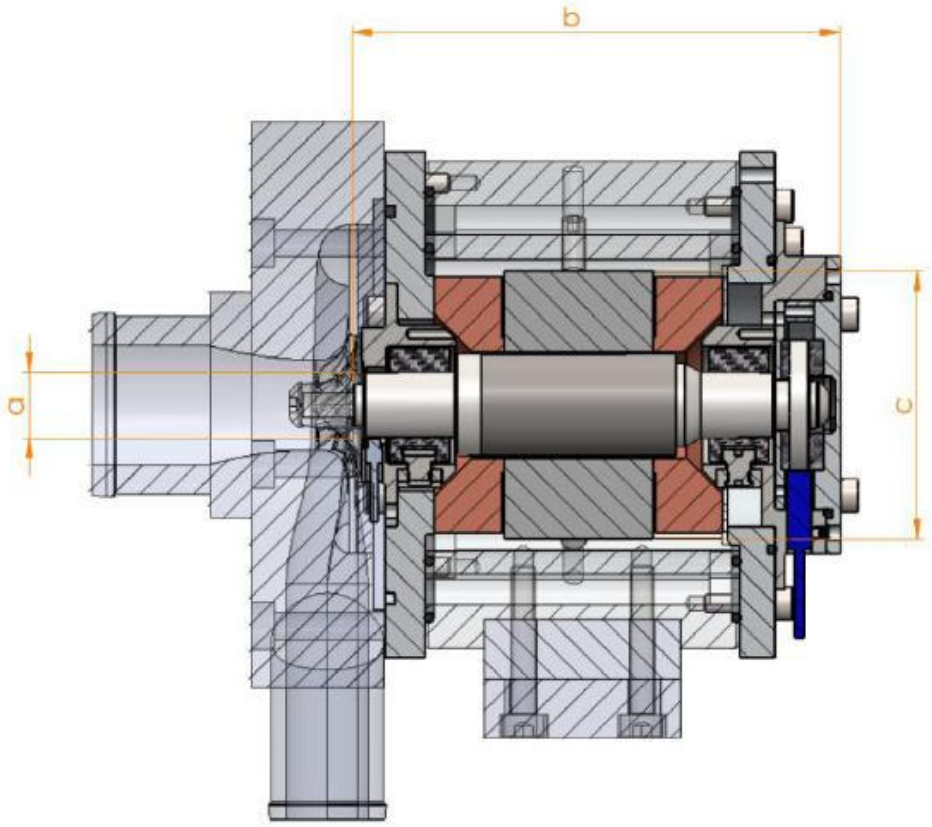

Fig 2.3 Measured motor design

3. TORQUE MEASUREMENT METHODS FOR VHS

Most of the torque measurement tools are made for machines with revolutions up to 50 krpm. Measuring machines with speed over 50 krpm is then problematic.

3.1 Two identical machines method

In [1], for 500,000 rpm, 100 W and 2 mNm drive system, a team of engineers used method of 2 identical machines on one common shaft, where one machine is as a drive motor and the second is a generator. Stator of motor is fixed to a frame of the test bench and generator's stator is held radially and axially with ball bearings and can rotate freely. On this stator is mounted a moment arm, which transfer moment into a force, which is measured with a force sensor.

3.2 Inertial method

Another method for measuring torque is the Inertial method, which is an indirect method based only on the inertia of a motor rotor. The position of the rotor is measured via coder, its frequency is related to acceleration of the rotor. Thanks to knowing the inertia I it is possible to obtain the torque T that must be delivered to rotor to produce the acceleration. An advantage of this method is that it is very fast and can be done for high torque values. Disadvantage is it cannot be done for continuous torque measurement. [5]

3.3 Eddy current brake method

Next method is based on the creation of braking torque in Eddy current brake with magnets on the motor shaft and then measuring it with a torque sensor. Because VHS machines have high power density, temperatures in the motor are critical. Advantage of Eddy current brake method is that it is contactless, so dissipated heat is created in the brake and does not go into the measured machine. This method was selected for this thesis for its simplicity. [5]

3.4 Ball bearing method

Team from Switzerland developed a new contactless method based on eddy currents as well. At the end of motor shaft are mounted multipolar axially magnetized permanent magnets. Over the airgap is on two ball bearings mounted a conductive shaft made of aluminum. Eddy currents are created in the conductive

shaft and causes the breaking torque. For the first measurement is the conductive shaft fixed, torque is measured, creating the slip curve. Then the conductive shaft is let to rotate freely and motor is driven at different speeds, creating second reaction torque. Speed of the conductive shaft is measured and second torque is then calculated. This method is more complex. [5]

4. EDDY CURRENT BRAKE DESIGN AND PRINCIPLE

The electromagnetic brake is a relatively primitive mechanism, yet it employs complex electromagnetic and thermal phenomena. As a result, the calculation of braking torque is a complex task.

4.1 Principle of Eddy current brake

According to Faraday's law of induction, when a conductor moves through a magnetic field or field moves through conductor, a change of a magnetic flux occurs and an electromotive force (EMF), thus electric currents, are induced in the conductive body, these currents are called Eddy currents. A closed-loop circuit appears in the depth of the conductor. Lenz's law states that a polarity of the induced EMF is such that it creates a current whose magnetic field is oriented against the change that produced it.

Faraday's law is given:

$$\varepsilon = \frac{d\Phi}{dt} = (\boldsymbol{v} \times \boldsymbol{B}) \cdot \boldsymbol{l}\,, \tag{4.1}$$

where ε is electromotive force, Φ is magnetic flux, $\boldsymbol{v}$ is vector of velocity, $\boldsymbol{B}$ is vector of magnetic flux density and $\boldsymbol{l}$ is vector of the length of an area which $\boldsymbol{B}$ penetrates.

The magnitude of Eddy current is:

$$I_{ed} = \frac{\varepsilon}{R} = \frac{1}{R} \cdot (\boldsymbol{v} \times \boldsymbol{B}) \cdot \boldsymbol{l}\,, \tag{4.2}$$

In this equation is R resistance of material of the conductor.

Another important variable, which occurs with higher frequency, is skin depth δ. Skin depth is defined as the depth below the conductor surface, where current density J exponentially drops to 37 % of surface value.

$$\delta = \sqrt{\frac{2}{\omega \cdot \mu_r \cdot \mu_0 \cdot \sigma}}, \tag{4.3}$$

where ω is angular speed, μ_r is relative permeability of material, μ_0 is permeability of vacuum and σ is conductivity of material.

Characteristics that might have effect on the conductive body moving in a magnetic field are:

a) Material

As given by equation (4.2), lower the resistance is, higher amplitude of eddy current could be achieved. Higher current amplitude means higher breaking force in eddy current brake. However ECB with PM has no regulation of magnetic flux B. It means higher the induced current in ECB is, stronger is reaction field, which is oriented against the PM magnetic flux and lowers it. Material also affects skin depth δ, as can be seen in formula (4.3).

b) Speed

Magnetic force exerted on an object moving through a magnetic field is higher with higher velocity of the object, as can be observed in equation (4.1). With higher speed is skin depth δ smaller, equation (4.3).

c) Direction

The direction of the electromotive force is given by Lenz's law. Maximum braking force can be achieved if vector of velocity $\boldsymbol{v}$ and vector of magnetic flux density $\boldsymbol{B}$ are perpendicular to each other, as can be seen in equation (4.1). [6]

4.2 Design and types of Eddy current brake

Eddy current brakes are composed of a magnetic flux source like permanent magnet or electromagnet separated from a conductor, which can be configured in a variety of forms including disks, drums, etc., usually made of copper or aluminum, by a small air gap. From the point of principle it doesn't matter, which part will be rotational, however from the design point of view it is preferable to have stationary magnetic flux source and disk connected to a rotating mechanical energy source. In this work because of great centrifugal forces is magnetic flux source rotating and brake is stationary, which is better from thermal point of view.

As is stated in [8], behind braking conductive material could be placed back iron for improving distribution of flux density and maximizing breaking power, therefore this option will be tested.

Eddy current brakes can be divided into two basic types: axial-flux and radial-flux.

4.2.1 Axial-flux Eddy current brakes

Their air gap is situated in radial direction. A closed circuit in which Eddy currents are induced has a disk shape, the brake usually includes two or more disks to enhance the braking effect and a set of coils disposed around the periphery of the disk.

1. Brake casing
2. Set of coils
3. Brake disk 1
4. Brake disk 2

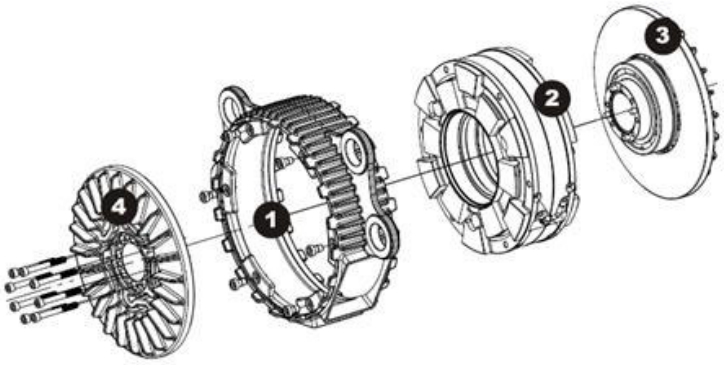

Fig 4.1 Configuration of axial-flux Eddy current brake [7]

4.2.2 Radial-flux Eddy current brakes

The air gap is formed in the axial direction. A closed circuit is a drum in whose cavity is an inserted coil or permanent magnet which generates an electromagnetic field. In this case, it is a more complex magnetic circuit that creates several poles of magnetic field with the use of one exciting coil.

1. Drum
2. Magnetic circuit
3. Coil

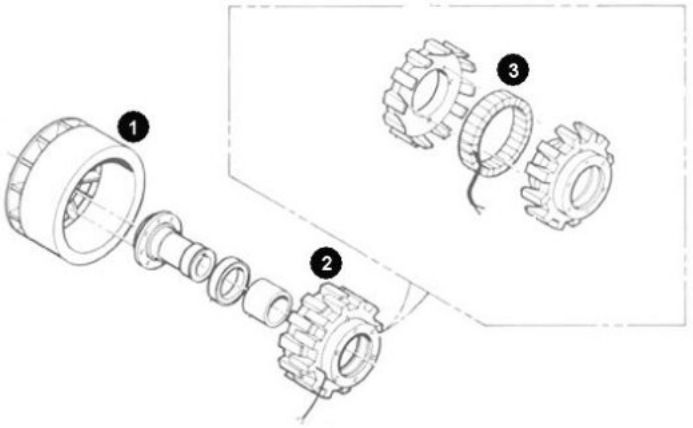

Fig 4.2 Configuration of radial-flux Eddy current brake [7]

For this thesis was chosen radial-flux Eddy current brake as a conductive drum with permanent magnets mounted on rotor shaft.

5. ANALYTICAL CALCULATION

5.1 Eddy current loss

Analytical calculation of Eddy currents in full material is very complex matter based on Maxwell's equations. The calculation will be based on literature [9] and [10]. Derivation of Eddy current loss is made under the assumption of a long massive cylinder with permeability μ and resistivity ρ, against which rotates magnetic field expressed by the intensity of magnetic field

$$H(x,t) = H_0 \cdot cos\left(\omega \cdot t - \frac{\pi}{\tau_p} \cdot x\right), \tag{5.1}$$

where

$$\tau_p = \pi \cdot \frac{D_C}{2} \cdot p \tag{5.2}$$

is pole pitch, D_C is inner diameter of conductive cylinder, p is number of poles of PM, ω is a slip angular velocity (in the case of ECB is slip velocity equal to synchronous angular velocity) and x is distance of origin of coordinates along the x axis. Assumption is that intensity of magnetic field has its components only in direction of x and y axis, whereas induced Eddy current density has component only in z axis.

Displacement currents for time-varying electromagnetic field calculation could be neglected, therefore displacement current density $\frac{\partial \boldsymbol{D}}{\partial t} = 0$. For linear environment with μ = konst. is according to Maxwell's equations

$$rot\ \boldsymbol{E} = -\mu \cdot \frac{\partial \boldsymbol{H}}{\partial t}, \tag{5.3}$$

$$rot\ \boldsymbol{H} = \boldsymbol{J}\ . \tag{5.4}$$

Where $\boldsymbol{E}$ indicates the electric field intensity vector, $\boldsymbol{H}$ is the magnetic field intensity vector, $\boldsymbol{J}$ is the current density vector and $\boldsymbol{D}$ is electric displacement field.

Further applies Ohm's law in differential form

$$\boldsymbol{E} = \rho \cdot \boldsymbol{J}\ . \tag{5.5}$$

Inserting equations (5.5) and (5.4) into (5.3) gives

$$rot\ rot\ \boldsymbol{H} = -\frac{\mu}{\rho} \cdot \frac{\partial \boldsymbol{H}}{\partial t}. \tag{5.6}$$

With respect to vortex principle of magnetic field applies $div\ \boldsymbol{H} = 0$, then

$$rot\ rot\ \boldsymbol{H} = grad\ div\ \boldsymbol{H} - \nabla^2 \boldsymbol{H} = -\nabla^2 \boldsymbol{H} = -\Delta \boldsymbol{H}. \tag{5.7}$$

By using equation (5.7) can be equation (5.6) written in components

$$\frac{\partial^2 H_x}{\partial x^2} + \frac{\partial^2 H_x}{\partial y^2} = \frac{\mu}{\rho} \cdot \frac{\partial H_x}{\partial t}. \tag{5.8}$$

$$\frac{\partial^2 \mathrm{H_y}}{\partial \mathrm{y}^2} + \frac{\partial^2 \mathrm{H_y}}{\partial \mathrm{x}^2} = \frac{\mu}{\rho} \cdot \frac{\partial \mathrm{H_y}}{\partial \mathrm{t}}. \tag{5.9}$$

As there are considered components of current density in x and y axis equal to zero ($J_x = 0$, $J_y = 0$), it is possible to express equation (5.4) only for component J_z

$$J_z = \frac{\partial H_y}{\partial x} - \frac{\partial H_x}{\partial y}. \tag{5.10}$$

If, on the brake surface ($y = 0$), the radial component of magnetic flux density B_y with the amplitude of B_{y0M} is given by the literature [10] by the equation

$$\begin{aligned} B_{y(y=0)} &= B_{y0M} \cdot \cos\left(\omega \cdot t - \frac{\pi}{\tau_p} \cdot x\right) = \\ &= B_{y0M} \cdot Re\left(e^{j\omega t} \cdot e^{-\frac{j\pi x}{\tau_p}}\right), \end{aligned} \tag{5.11}$$

then solution for brake ($y > 0$) could be assumed according to (5.9)

$$\begin{aligned} H_y &= H_{y0M} \cdot \cos\left(\omega \cdot t - \frac{\pi}{\tau_p} \cdot x - \beta_k \cdot y\right) = \\ &= H_{y0M} \cdot Re\left(e^{j\omega t} \cdot e^{-\frac{j\pi x}{\tau_p}} \cdot e^{-j\beta_k y}\right), \end{aligned} \tag{5.12}$$

where β_k is unknown coefficient, which must be calculated.

Inserting (5.12) into (5.9) gives

$$-H_{y0M}\cdot\beta_k^2\cdot\cos\left(\omega\cdot t-\frac{\pi}{\tau_p}\cdot x-\beta_k\cdot y\right)-H_{y0M}\cdot\left(\frac{\pi}{\tau_p}\right)^2 \tag{5.13}$$
$$\cdot\cos\left(\omega\cdot t-\frac{\pi}{\tau_p}\cdot x-\beta_k\cdot y\right)=$$
$$=-\frac{\mu}{\rho}\cdot H_{y0M}\cdot\omega$$
$$\cdot\sin\left(\omega\cdot t-\frac{\pi}{\tau_p}\cdot x-\beta_k\cdot y\right).$$

After modifying can be got

$$\beta_k^2+\left(\frac{\pi}{\tau_p}\right)^2=-j\cdot\frac{\mu}{\rho}\cdot\omega\,. \tag{5.14}$$

Unknown coefficient β_k is then a complex number, which can be expressed as

$$\beta_k=\beta_{ka}-j\beta_{kb}\,. \tag{5.15}$$

After inserting into equation (5.14) can be obtained system of equations

$$\beta_{ka}^2-\beta_{kb}^2=-\left(\frac{\pi}{\tau_p}\right)^2, \tag{5.16}$$

$$2\cdot\beta_{ka}\cdot\beta_{kb}=\frac{\mu}{\rho}\cdot\omega=\omega\cdot\mu\cdot\sigma\,. \tag{5.17}$$

By solving these equations are reached real and imaginary components of coefficient β_k

$$\beta_{ka}=\sqrt{-\frac{1}{2}\cdot\left(\frac{\pi}{\tau_p}\right)^2+\sqrt{\frac{1}{4}\cdot\left[\left(\frac{\pi}{\tau_p}\right)^4+\omega^2\cdot\mu^2\cdot\sigma^2\right]}}. \tag{5.18}$$

$$\beta_{kb}=\sqrt{+\frac{1}{2}\cdot\left(\frac{\pi}{\tau_p}\right)^2+\sqrt{\frac{1}{4}\cdot\left[\left(\frac{\pi}{\tau_p}\right)^4+\omega^2\cdot\mu^2\cdot\sigma^2\right]}}. \tag{5.19}$$

If the material where are induced Eddy currents has permeability $\mu_r > 1000$ (for instance ferromagnetic), then often applies

$$\left(\frac{\pi}{\tau_p}\right)^2 \ll \omega \cdot \mu \cdot \sigma \,, \tag{5.20}$$

and then equations (5.18) and (5.19) could be simplified

$$\beta_{ka} = \beta_{kb} = \sqrt{\frac{\omega \cdot \mu \cdot \sigma}{2}}\,, \tag{5.21}$$

which is the reciprocal of the equivalent depth of penetration (skin depth).

The condition (5.20) is not met with conductive material like copper or aluminum, hence it is necessary to calculate with real and imaginary component of coefficient β_k in full form as is stated in (5.18) and (5.19).

Equation (5.12) for magnetic field intensity gets form

$$\begin{aligned} H_y = H_{y0M} \cdot Re\left(e^{j\omega t} \cdot e^{-\frac{j\pi x}{\tau_p}} \cdot e^{-j(\beta_{ka} - j\beta_{kb})y}\right) = \\ = H_{y0M} \cdot e^{-j\beta_{kb}y} \\ \cdot \cos\left(\omega \cdot t - \frac{\pi}{\tau_p} \cdot x - \beta_{ka} \cdot y\right). \end{aligned} \tag{5.22}$$

With assumption zero magnitude of magnetic field intensity component in z axis direction ($H_z = 0$), applies equation

$$div\, \boldsymbol{H} = \frac{\partial H_x}{\partial x} + \frac{\partial H_y}{\partial y} = 0\,, \tag{5.23}$$

then it is possible to express magnetic field intensity component H_x in x axis direction

$$H_x = -\int \frac{\partial H_y}{\partial y} dx\,. \tag{5.24}$$

After inserting (5.22) into (5.24) can be obtained H_x in x axis direction

$$H_x = -\int \frac{\partial H_y}{\partial y}\,dx = \tag{5.25}$$
$$= -\int H_{y0M} \cdot e^{-\beta_{kb} y} \cdot \left[-\beta_{kb} \cdot \cos\left(\omega \cdot t - \frac{\pi}{\tau_p} \cdot x - \beta_{ka} \cdot y\right) + \beta_{ka} \cdot \sin\left(\omega \cdot t - \frac{\pi}{\tau_p} \cdot x - \beta_{ka} \cdot y\right)\right] dx =$$
$$= -H_{y0M} \cdot e^{-\beta_{kb} y} \cdot \left[\beta_{kb} \cdot \frac{\tau_p}{\pi} \cdot \sin\left(\omega \cdot t - \frac{\pi}{\tau_p} \cdot x - \beta_{ka} \cdot y\right) + \beta_{ka} \cdot \frac{\tau_p}{\pi} \cdot \cos\left(\omega \cdot t - \frac{\pi}{\tau_p} \cdot x - \beta_{ka} \cdot y\right)\right].$$

Calculation of current density J_z is made according to (5.10)

$$\frac{\partial H_x}{\partial y} = -H_{y0M} \cdot \frac{\tau_p}{\pi} \cdot e^{-\beta_{kb} y} \cdot \left[-{\beta_{kb}}^2 \cdot \sin\left(\omega \cdot t - \frac{\pi}{\tau_p} \cdot x - \beta_{ka} \cdot y\right) - 2 \cdot \beta_{ka} \cdot \beta_{kb} \cdot \cos\left(\omega \cdot t - \frac{\pi}{\tau_p} \cdot x - \beta_{ka} \cdot y\right) + {\beta_{ka}}^2 \cdot \sin\left(\omega \cdot t - \frac{\pi}{\tau_p} \cdot x - \beta_{ka} \cdot y\right)\right] \tag{5.26}$$

$$\frac{\partial H_y}{\partial x} = H_{y0M} \cdot \frac{\tau_p}{\pi} \cdot e^{-\beta_{kb} y} \cdot \sin\left(\omega \cdot t - \frac{\pi}{\tau_p} \cdot x - \beta_{ka} \cdot y\right), \tag{5.27}$$

then current density J_z is after editing

$$J_z = \frac{\partial H_y}{\partial x} - \frac{\partial H_x}{\partial y} = \tag{5.28}$$
$$= H_{y0M} \cdot e^{-\beta_{kb} y} \cdot \left(\frac{\pi}{\tau_p} - {\beta_{kb}}^2 \cdot \frac{\tau_p}{\pi} + {\beta_{ka}}^2 \cdot \frac{\tau_p}{\pi} \right) \cdot \sin\left(\omega \cdot t - \frac{\pi}{\tau_p} \cdot x - \beta_{ka} \cdot y \right) - H_{y0M} \cdot e^{-\beta_{kb} y} \cdot \left(2 \cdot \beta_{ka} \cdot \beta_{kb} \cdot \frac{\tau_p}{\pi} \right) \cdot \cos\left(\omega \cdot t - \frac{\pi}{\tau_p} \cdot x - \beta_{ka} \cdot y \right).$$

For Eddy current loss calculation it is not necessary to know exact distribution of current density in material. It is sufficient to know effective value of current density in dependence on *y* axis. Although the distribution of the current density at a certain depth *y* over the periphery of the rotor changes, its effective value is constant in this layer. Effective value of current density could be obtained from amplitude

$$J_{zM} = \tag{5.29}$$
$$= H_{y0M} \cdot e^{-\beta_{kb} y} \cdot \sqrt{\left(\frac{\pi}{\tau_p} - {\beta_{kb}}^2 \cdot \frac{\tau_p}{\pi} + {\beta_{ka}}^2 \cdot \frac{\tau_p}{\pi} \right)^2 + \left(-2 \cdot \beta_{ka} \cdot \beta_{kb} \cdot \frac{\tau_p}{\pi} \right)^2}.$$

Eddy current loss per unit of area [W·m^{-2}], when considering width of material *h* in the *y* axis direction, can be calculated using the equation

$$\Delta p_{ed} = \frac{1}{\sigma} \cdot \int_0^h \left(\frac{J_{zM}}{\sqrt{2}} \right)^2 dy \tag{5.30}$$
$$= -\frac{1}{4 \cdot \sigma \cdot \beta_{kb}} \cdot {H_{y0M}}^2 \cdot \left[\left(\frac{\pi}{\tau_p} - {\beta_{kb}}^2 \cdot \frac{\tau_p}{\pi} + {\beta_{ka}}^2 \cdot \frac{\tau_p}{\pi} \right)^2 + \left(-2 \cdot \beta_{ka} \cdot \beta_{kb} \cdot \frac{\tau_p}{\pi} \right)^2 \right] \cdot \left[e^{-2 \cdot \beta_{kb} \cdot h} - 1 \right].$$

If the inner surface of the conductor layer is

$$S_c = \pi \cdot D_C \cdot l_C\,, \tag{5.31}$$

where l_C is adjusted length of conductor, which is given

$$l_C = l_{PM} + 2 \cdot \delta \,. \tag{5.32}$$

Since conductor is longer than permanent magnet, part of magnetic flux enter conductor in close proximity to the magnet, it is respected by increasing conductor's length in equation by twice the length of the air gap. Then Eddy current loss in conductor is

$$\begin{aligned} \Delta P_{edC} = -\pi \cdot D_C \cdot l_C \cdot \frac{1}{4 \cdot \sigma_{C\vartheta} \cdot \beta_{kbC}} \cdot \left(\frac{B_{yCM}}{\mu_0 \cdot \mu_{rC}}\right)^2 \\ \cdot \left[\left(\frac{\pi}{\tau_p} - {\beta_{kbC}}^2 \cdot \frac{\tau_p}{\pi} + {\beta_{kaC}}^2 \cdot \frac{\tau_p}{\pi}\right)^2 \right. \\ \left. + \left(-2 \cdot \beta_{kaC} \cdot \beta_{kbC} \cdot \frac{\tau_p}{\pi}\right)^2\right] \\ \cdot \left[e^{-2 \cdot \beta_{kbC} \cdot h_C} - 1\right], \end{aligned} \tag{5.33}$$

where index C stands for conductor, D_C and h_C is inner diameter and width of conductive material, ϑ stands for temperature effect. Amplitude of the magnetic flux density on the surface of the conductor B_{yCM} is changing in dependence on rotational speed ω of PM and used brake material. Its value for certain speed and conductor is taken from Ansys Maxwell 2D.

Losses in conductor and back iron are calculated separately. Losses in conductor are dominant, it is given by higher value of magnetic flux density, which by passing through conductor in y axis direction decreases exponentially. Amplitude of magnetic flux density on the surface of back iron can be described by equation

$$B_{yFeM} = B_{yCM} \cdot e^{-\beta_{kbC} \cdot h_C} \,. \tag{5.34}$$

Eddy current losses in back iron can be expressed by equation

$$\begin{aligned} \Delta P_{edFe} = -\pi \cdot D_{Fe} \cdot l_C \cdot \frac{1}{4 \cdot \sigma_{Fe\vartheta} \cdot \beta_{kbFe}} \cdot \left(\frac{B_{yFeM}}{\mu_0 \cdot \mu_{rFe}}\right)^2 \\ \cdot \left[\left(\frac{\pi}{\tau_p} - {\beta_{kbFe}}^2 \cdot \frac{\tau_p}{\pi} + {\beta_{kaFe}}^2 \cdot \frac{\tau_p}{\pi}\right)^2 \right. \\ \left. + \left(-2 \cdot \beta_{kaFe} \cdot \beta_{kbFe} \cdot \frac{\tau_p}{\pi}\right)^2\right] \\ \cdot \left[e^{-2 \cdot \beta_{kbFe} \cdot h_C} - 1\right], \end{aligned} \tag{5.35}$$

where D_{Fe} is inner diameter of back iron.

Windage loss were calculated as well, but its value is negligible.

6. FEM MODEL OF EDDY CURRENT BRAKE IN FEMM AND ANSYS MAXWELL

Analytical calculation made in chapter 5. is important for understanding basic relations and dependencies between individual parameters. Its advantage is fast calculation, but a number of simplifications is disadvantage, which affect the accuracy of the result. For these reasons, finite element method (FEM) is used, in particular to clarify the calculated parameters of ECB and to assess the analytical calculation. FEM disadvantage is its calculation duration.

Since measurement of torque takes a lot of time, ECB's temperature is high. All simulation are made for this temperature: 140 °C. This affect material's conductivity and PM's magnetic coercivity.

According to initial simulations in the beginning of the thesis were made several prototypes of ECB, which are going to be measured and compared to analytical calculation and detailed simulations. Goal is to find out if its features are sufficient for proper torque measurement. Example of its dimensions and properties are shown in Fig 6.1.

PM thickness	2,7	mm
PM outer diameter	12,3	mm
PM length	6,25	mm
sleeve diameter	14	mm
brake inner diameter	16	mm
brake outer diameter	18	mm
back iron outer diameter	24	mm
brake length	20	mm
brake material	aluminum	-
brake material conductivity at 20 °C	34	MS/m
back iron material	Steel C45	-
back iron conductivity at 20 °C	7	MS/m
PM material	NdFe42UH	-
PM coercitivity at 20 °C	-970000	A/m
Coercivity temperature drop	-0,10	%/°C
number of poles	2	-
steel relative permeability	1000	-

Fig 6.1 Table of prototype ECB dimensions and properties

Brake length is 20 mm due to need of mounting a torque sensor shaft.

Two main materials will be in consideration, copper with conductivity set on 39,5 MS/m and aluminum with conductivity 23 MS/m, as was stated before, these conductivities are lower because of temperature. Several brake widths are tested to find out ideal one for maximum braking power. Conductivity of back iron (BI), 5,2 MS/m, is adjusted for temperature as well.

6.1 Finite element method magnetic

A finite element model (FEM) of the Eddy current brake was first created in software Finite element method magnetic (FEMM) with following simplifying assumptions:

1. The rotating magnet on rotor is spread into the plane and replaced by two layers of static windings with a phase shift between the currents in the layers, whole design can be seen in Fig 6.2. One layer has inside real component of current and the second has imaginary component of current. To simulate magnetic flux in airgap as sinusoid as it is created by real parallel magnetized magnet, the winding had to be separated to smaller pieces with different amplitudes of current inside, on the sides of whole design the periodic boundary condition had to be used. To complete the simulation, the winding must be spatially shifted in the layers, which together with phase shift simulates the movement of the magnet. The problem becomes a static time-harmonic problem. Example of such winding can be observed in Fig 6.3.
2. The current value is chosen so that the first harmonic of the flux density due to the currents is equal to the first harmonic of the flux density due to the brake permanent magnet.

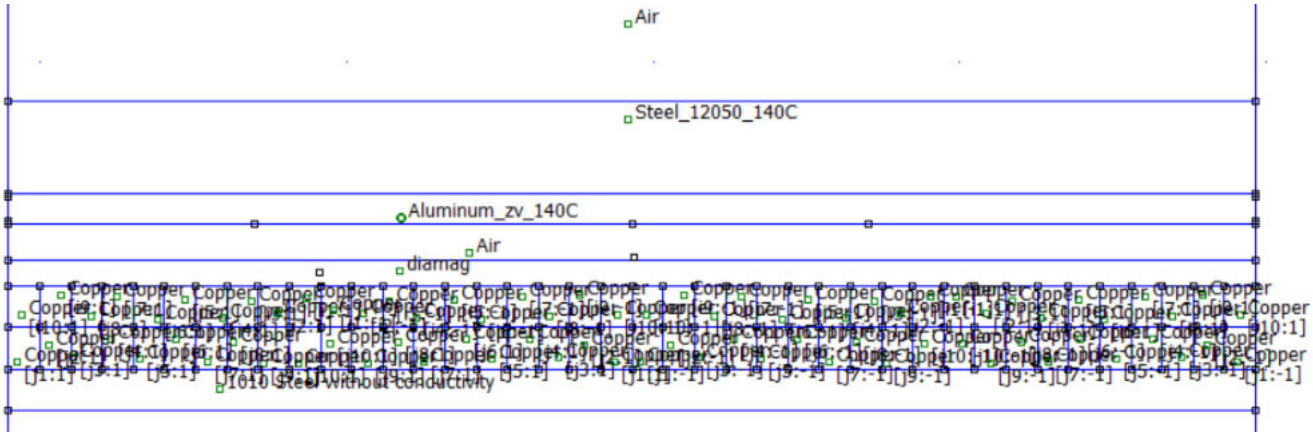

Fig 6.2 Design of ECB with periodic boundary conditions and winding simulating PM

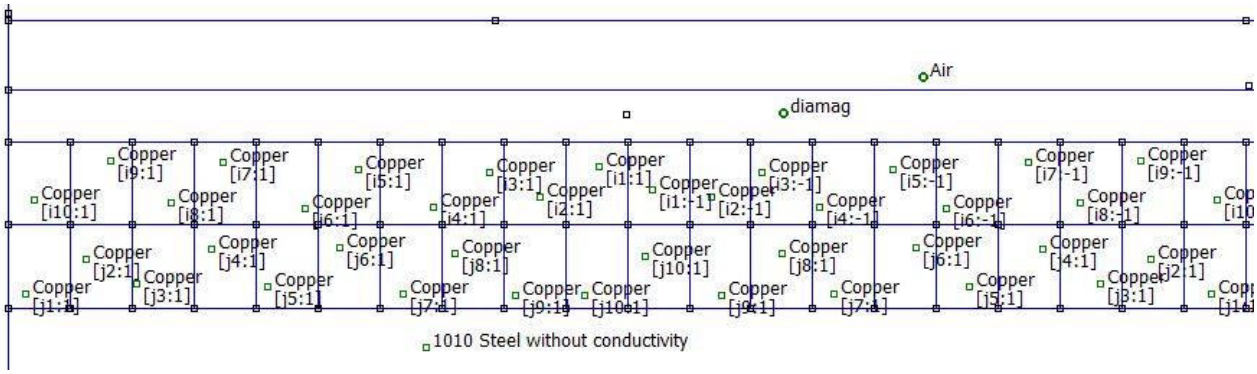

Fig 6.3 Detail of winding for PM flux simulation

In Fig 6.4 is shown the flux density in airgap created by currents in winding. Maximum reaches 0,22 T, the same value as permanent magnet.

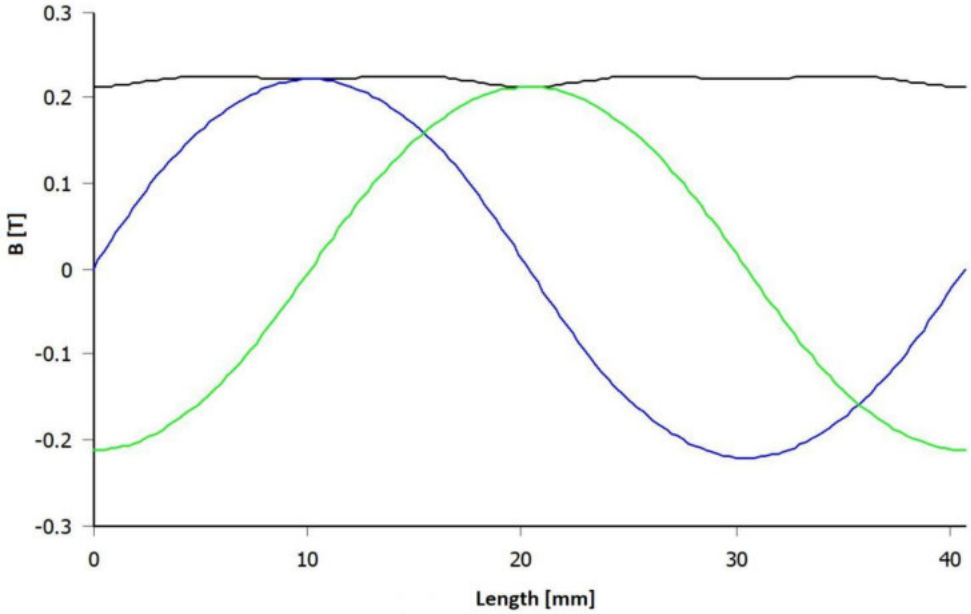

Fig 6.4 Flux density in airgap of ECB at 1 Hz

Example of FEMM current density distribution in ECB for 100 krpm, Al conductor, could be observed in Fig 6.5.

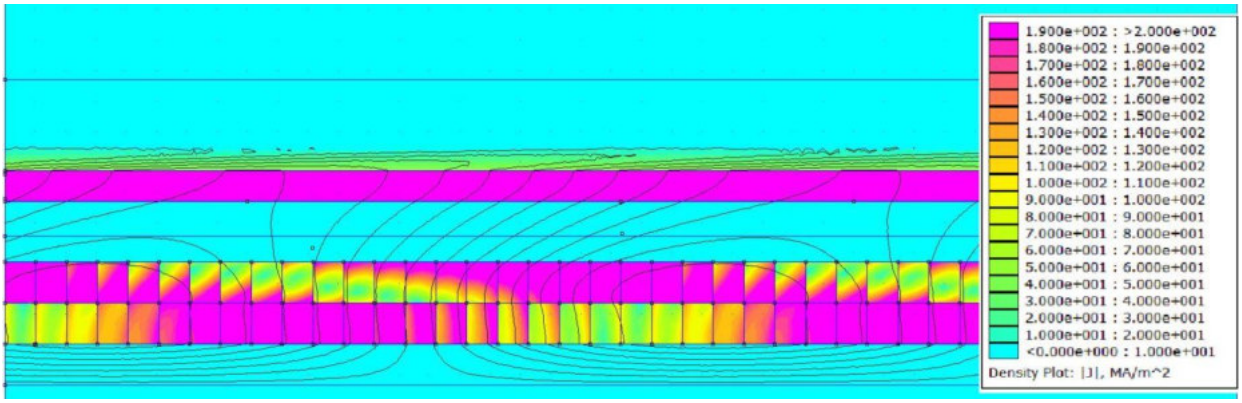

Fig 6.5 Distribution of current density in Aluminum ECB, 100 krpm.

6.2 FEM in Ansys Maxwell

Simulation of braking system was created also in program Ansys Maxwell 2D version 2017. Although 3D would be much more suitable for Eddy current simulation in ECB, where permanent magnet is shorter than conductive body, its calculation is too time consuming. 3D simulations were made only for the most up-to-date dimensions and materials.

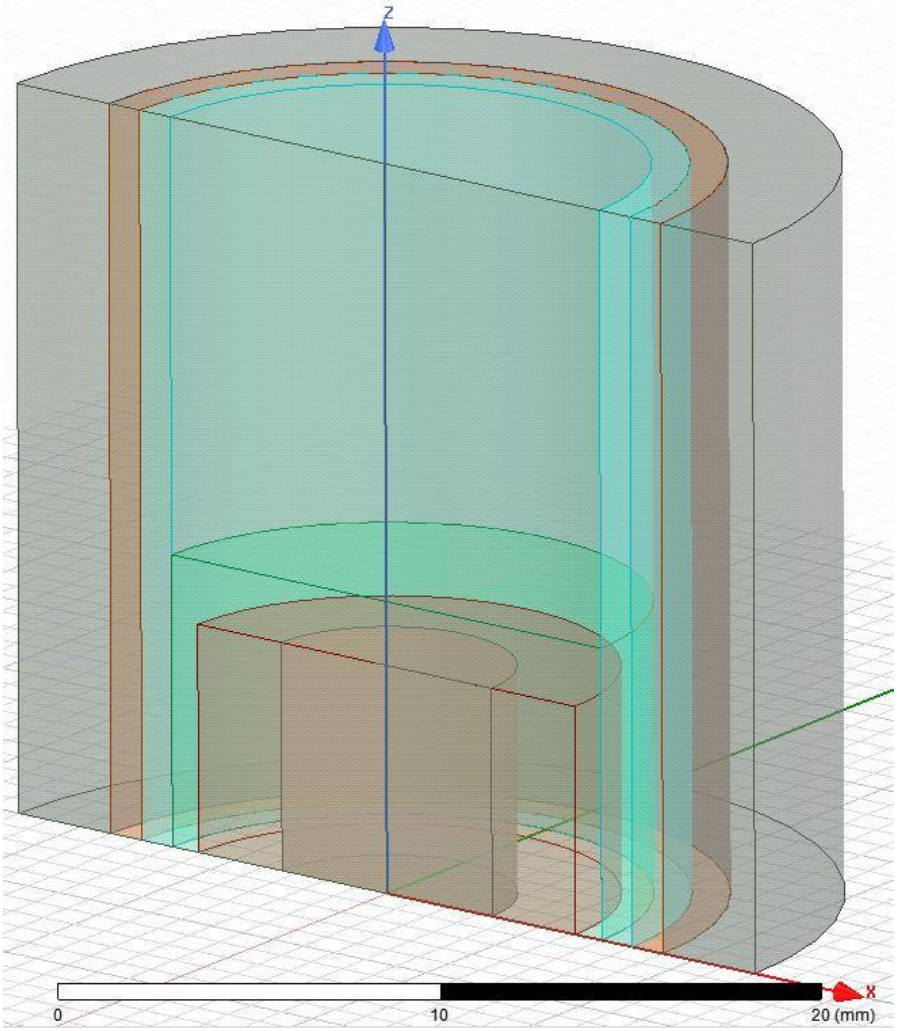

Fig 6.6 Design of 3D FEM model of ECB

Since ECB is a two pole machine, it can be divided into half thanks to Master and Slave boundary condition and thus reduce its computation time. In the middle of airgap is assigned band around rotating parts (green cylinder in Fig 6.6). ECB structure is depicted in Fig 6.7 as Ansys 2D model. From right to left is as follows: back iron, brake conductor, airgap, band, PM, rotor steel.

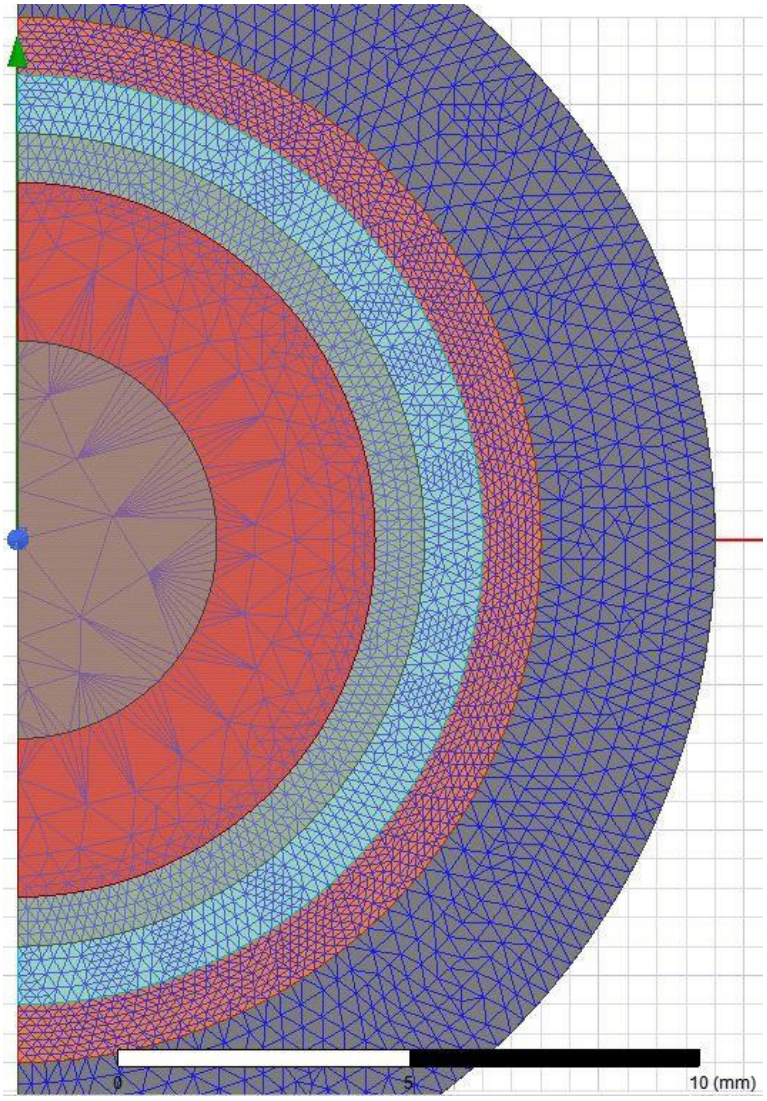

Fig 6.7 Assigned mesh operations on different parts of 2D model

Into all models were assigned nonlinear B-H characteristics of ferromagnetic materials (Back iron is made of Steel 12050 (Steel C45)) and its conductivities. Mesh element size is smaller in area of airgap, band, conductor and back iron. Eddy current loss calculation is assigned to conductor and back iron. Time step of simulation is chosen 200 steps per revolution and stop time is set on 0,01 ms after transient process has disappeared.

The distribution of magnetic flux density in the aluminum ECB under the load of 100 krpm is shown in Fig 6.8 for time 0,01 ms from the beginning of the simulation. An effect of Eddy currents is obvious in the back iron, which is made of solid steel. Magnetic flux density is clearly deformed and surface layer of back iron is oversaturated.

In Fig 6.10 is depicted current density distribution in ECB under the load. It can be seen that currents are not only in conductor drum, but also in inner layers of back iron. Due to high frequency, thus skin depth, aren't currents in the whole back iron.

As can be seen in Fig 6.9, loss density distribution in ECB is very influenced by current distribution and skin depth, most of the losses are created in conductor drum, but also in back iron.

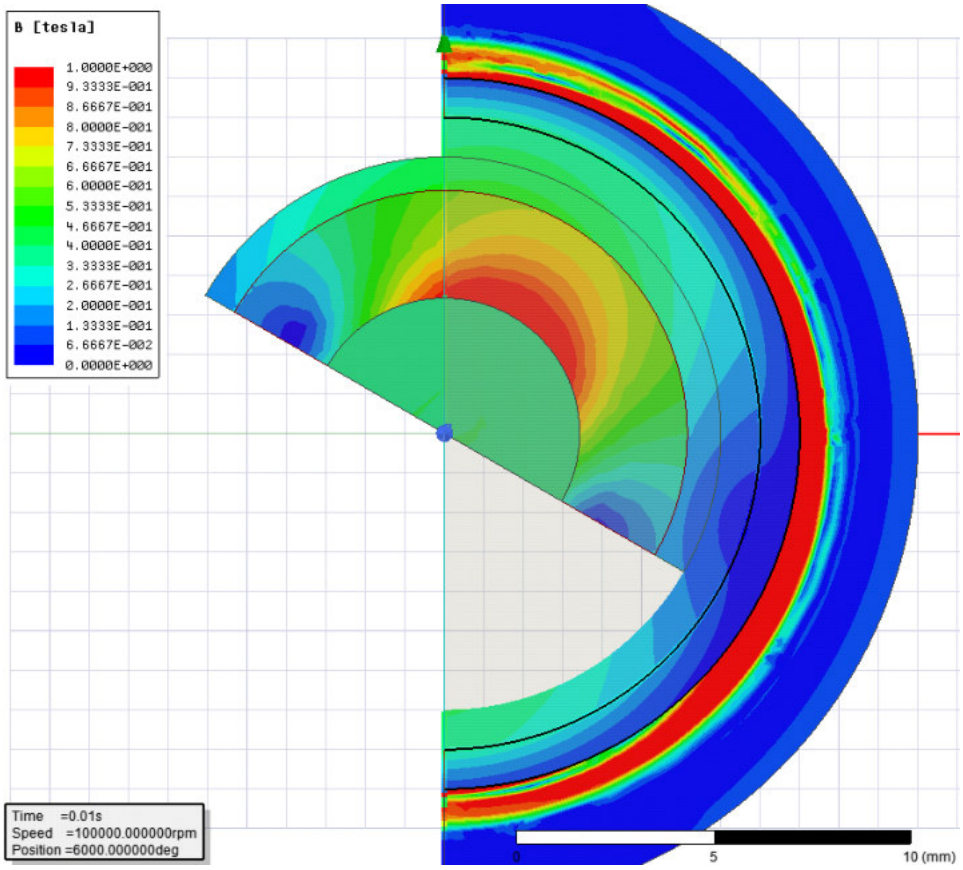

Fig 6.8 The distribution of magnetic flux density in ECB for Al conductor, n = 100 krpm

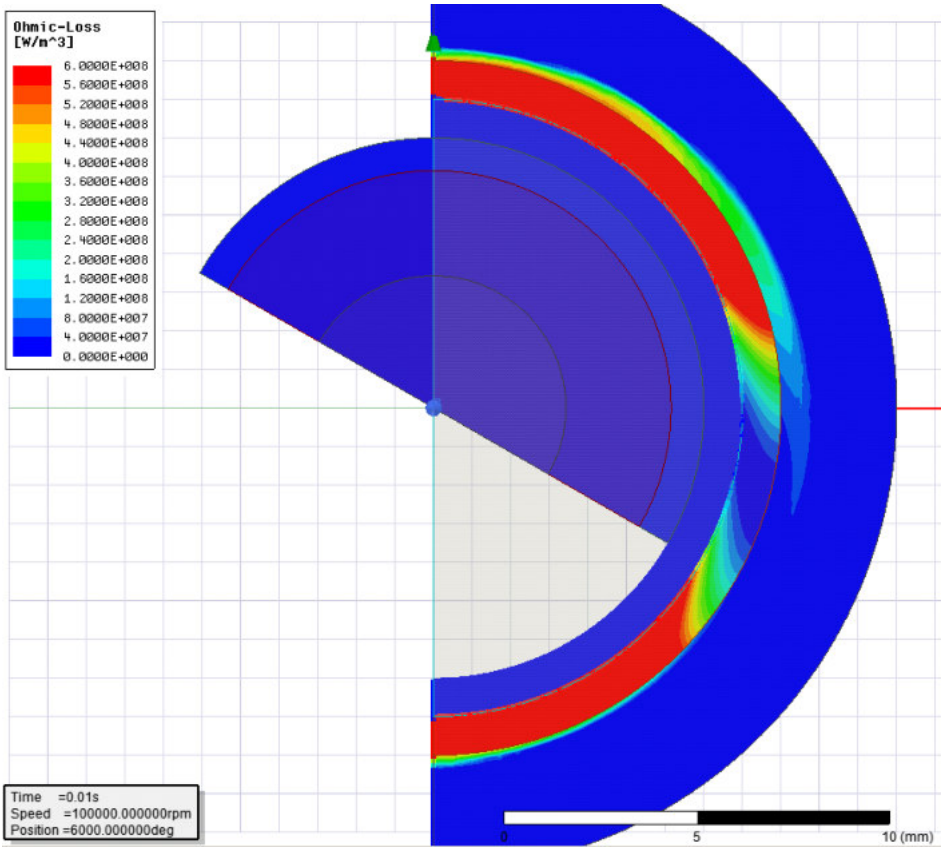

Fig 6.9 The distribution of volume loss density in ECB for Al conductor, n = 100 krpm

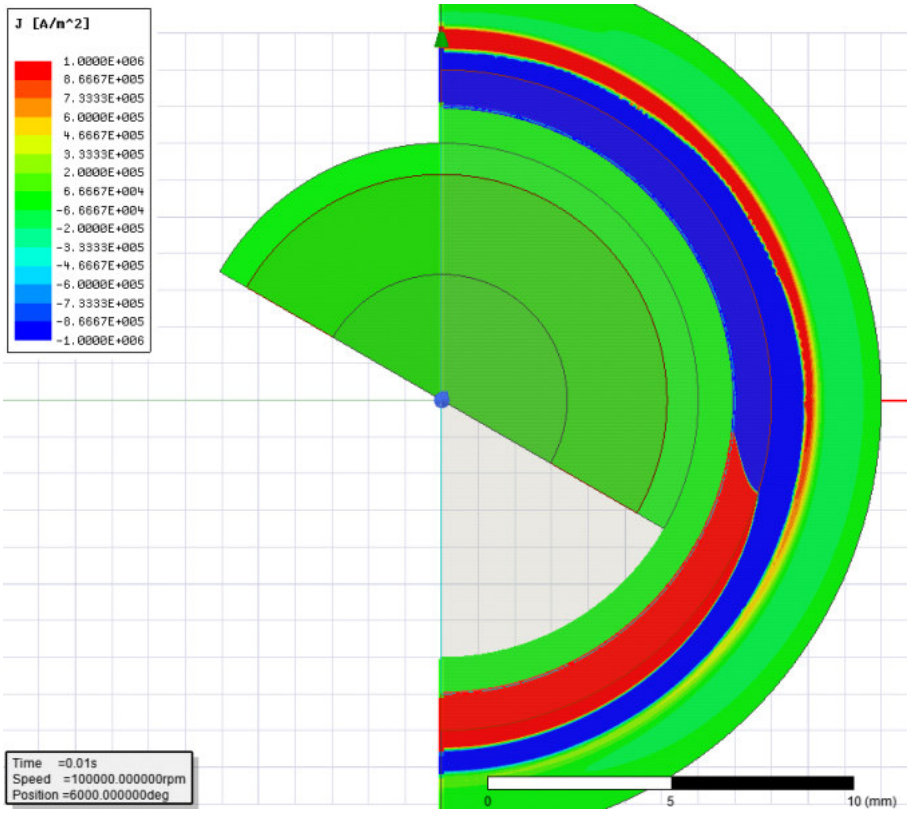

Fig 6.10 The distribution of current density in ECB for Al conductor, n = 100 krpm

7. MEASUREMENT

To verify the results from the calculation and simulations, several measurements of the VHS were made. Because manufactory of ECB takes a lot of time, a prototype of ECB was made, according to initial simulations and materials in stock, in the beginning of thesis. Its features and dimensions are shown in Fig 6.1. Tested were two conductor drums: copper and aluminum, with several brake widths: 1 – 3 mm, more has been shown as not efficient. Speed range is from 50 to 200 krpm.

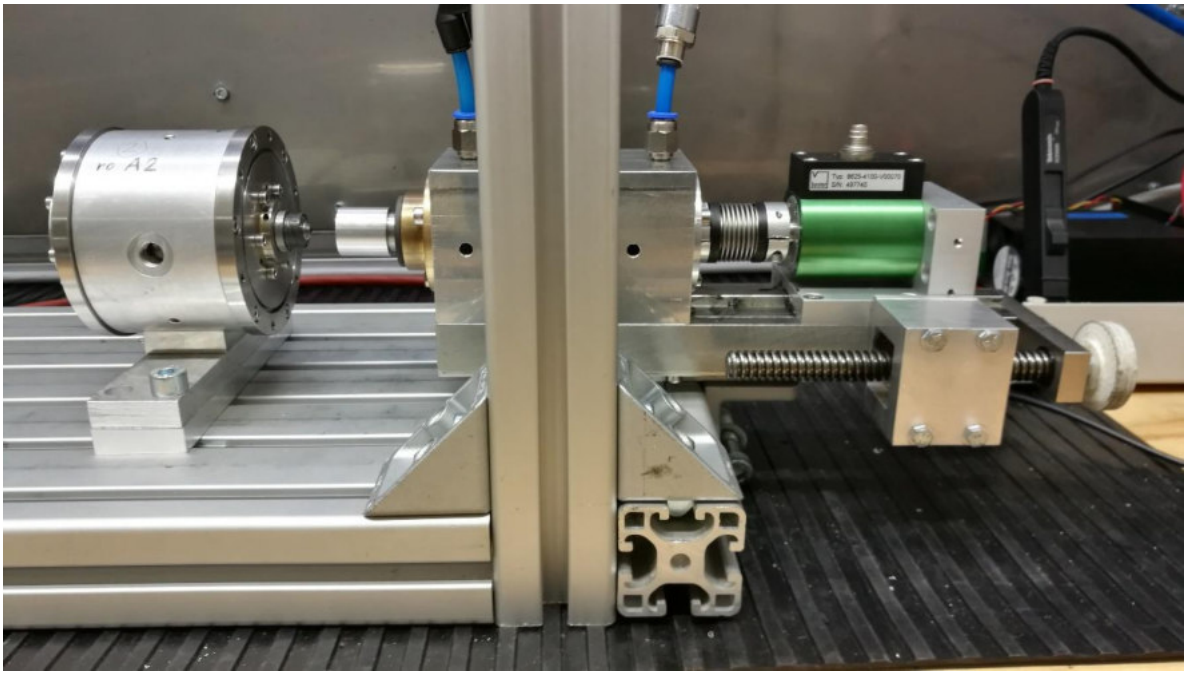

Fig 7.1 Measurement stand for ECB prototype

In Fig 7.1 you can see the measurement stand. Closer look at the brake is in Fig 7.2 and examples of some other ECB prototypes are in Fig 7.3. Measured VHS motor on the left, aluminum ECB mounted on freely rotating shaft on aerostatic bearings in order not to radially load the high precision torque sensor on the right. Forced air cooling is provided by means of air nozzles directed against the ECB.

List of used measurement devices:

- Burster Torque Sensor 8625-4100-V00070, S. no. 497740
- Power supply EA-PS 8360-10 T, S. no. 1544310001
- Zhaoxin DC power supply RXN-1503D, S. no. A02881
- Tektronix TDS 2004C Oscilloscope, S. no. TDS2004C C011868
- Tektronix P5200A Differential Probe, S. no. P5200A C024993
- Sobriety TensoAmp TA-01 Measurement Transducer, S. no. S-TA-01-004
- Lutron TM-902C Digital Thermometer, S. no. 201213341

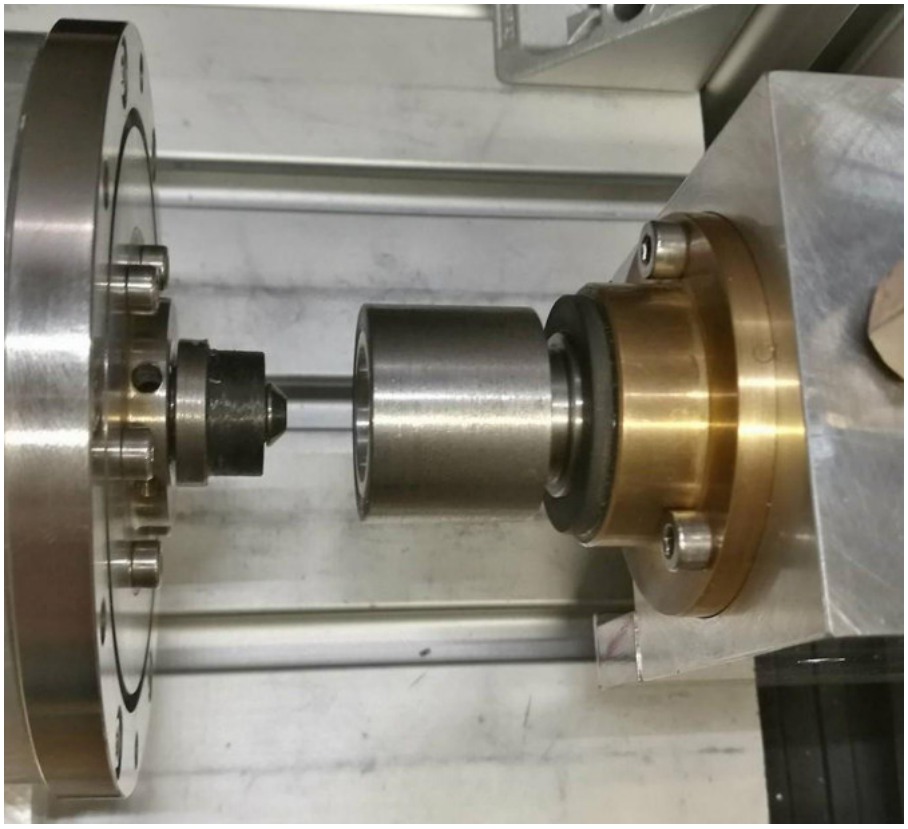

Fig 7.2 Detail of PM and aluminum ECB

Fig 7.3 Example of some ECBs

8. RESULTS COMPARISION

Simulations and measurement were made for several values of speed: 50, 100, 150 and 200 krpm. The purpose is to find out if the prototype is capable of creating enough braking power to measure VHS. The limits are as follows: for 50 krpm is sufficient braking power 170 W. For 100 krpm: 330 W. For 150 krpm: 500 W. For 200 krpm: 670 W.

8.1 Results for 50 krpm

In Table 8.1 are shown results from simulation in FEMM and Ansys/Maxwell, analytical calculation and measurement. Shown is also normal of magnetic flux density on the surface of conductive drum B_{yCM}, taken from Ansys/Maxwell 2D, used in analytical calculation.

50 krpm	brake width	B_{yCM}	FEMM	Ansys	Calculation	Measurement
			ΔP_{ed_FEMM}	ΔP_{ed_Ansys}	ΔP_{ed_cal}	ΔP_{ed_meas}
	[mm]	[T]	[W]	[W]	[W]	[W]
Cu	3	0,069	78	95	84	76
Cu	2	0,08	110	135	100	115
Cu	1	0,15	195	265	239	272
Al	3	0,095	114	140	111	117
Al	2	0,128	160	210	169	207
Al	1	0,22	240	350	330	373

Table 8.1 Comparison of measured losses in ECB at speed 50 krpm with simulations in FEMM and Ansys Maxwell 2D and analytical calculation

Dependency of Eddy current losses (braking power) on brake conductor width are displayed in graphical form in Fig 8.2 for copper and Fig 8.1 for aluminum. It can be seen that aluminum, less conductivity, reaches higher losses. Reasons are greater skin depth of aluminum, thus better current density distribution, and higher values of normal magnetic flux density B_{yCM}. Curves from Ansys, analytical calculation and measurement are almost identical, except FEMM curve, which differs at 1 mm brake width. It can be caused by simplifications of the model in FEMM, which uses copper winding with chosen currents instead of permanent magnet, its behavior could be slightly different. Possible improvement of FEMM model could be use of equivalent current density equation written in Source current density in Block property, as can be seen in [11], instead of using two layers of winding.

It turned out that the ECB losses for 50 krpm are sufficient to measure the torque.

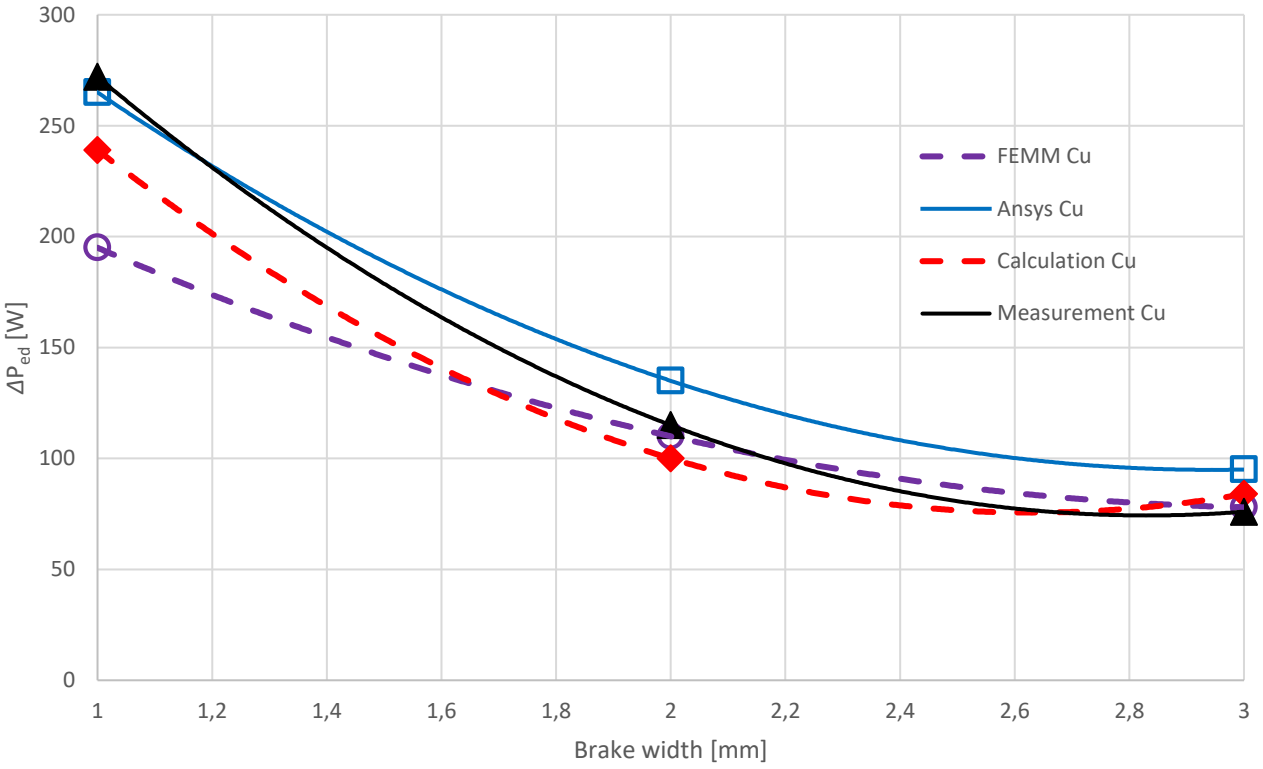

Fig 8.2 Braking power in copper ECB versus width of conductor at 50 krpm

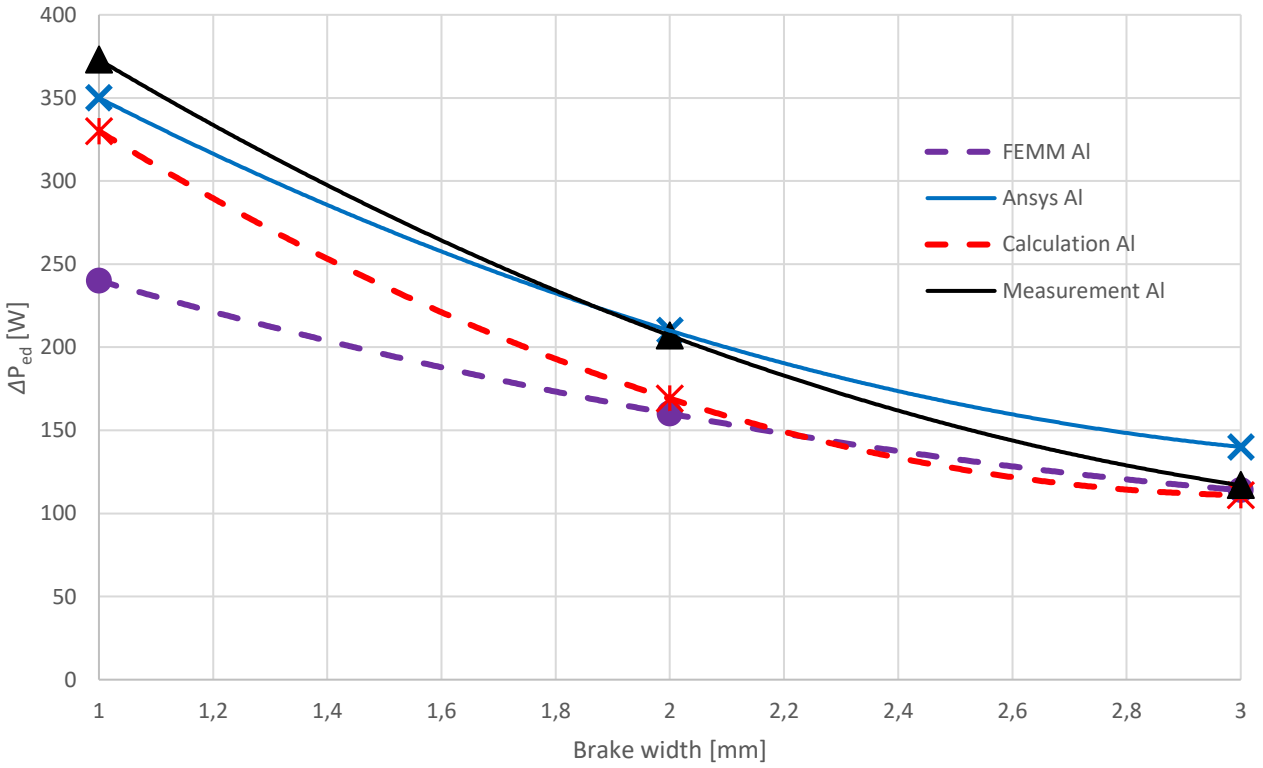

Fig 8.1 Braking power in aluminum ECB versus width of conductor at 50 krpm

8.2 Results for 100 krpm

100 krpm	brake width	B_{yCM}	FEMM	Ansys	Calculation	Measurement
			ΔP_{ed_FEMM}	ΔP_{ed_Ansys}	ΔP_{ed_cal}	ΔP_{ed_meas}
	[mm]	[T]	[W]	[W]	[W]	[W]
Cu	3	0,051	102	125	141	111
Cu	2	0,053	124	150	142	166
Cu	1	0,08	230	290	238	355
Al	3	0,064	140	170	159	144
Al	2	0,072	190	230	181	249
Al	1	0,13	340	455	416	505

Table 8.2 Comparison of measured losses in ECB at speed 100 krpm with simulations in FEMM and Ansys Maxwell 2D and analytical calculation

In Table 8.2 could be observed results of simulations, calculation and measurement for 100 krpm. Graphical form of dependencies of Eddy current losses on brake width are depicted in Fig 8.3 and Fig 8.4. It can be observed, that FEMM simulation results are now closer to the other curves. Eddy current losses results for 1 mm brake width from measurement have significant difference from Ansys simulation or calculation. It is done by rise of temperature, which is for 3 mm lower and for 1 mm, which is warmed up much faster, higher. Improvement could be in adjusting conductivity for exact temperature for different types of brake widths and materials. Problem is that measuring the temperature while loading is due to lack of space very difficult. Another reason is that both the simulations and the calculation are 2D and consider induced currents only in the *z* axis, but in real case is magnet shorter than ECB, thus Eddy currents can go further into *z* axis and at some point they have to turn and go in *x* and *y* axis as well, then they turn again and go back. These effects increase the value of losses.

It turned out that the ECB losses for 100 krpm are sufficient to measure the torque.

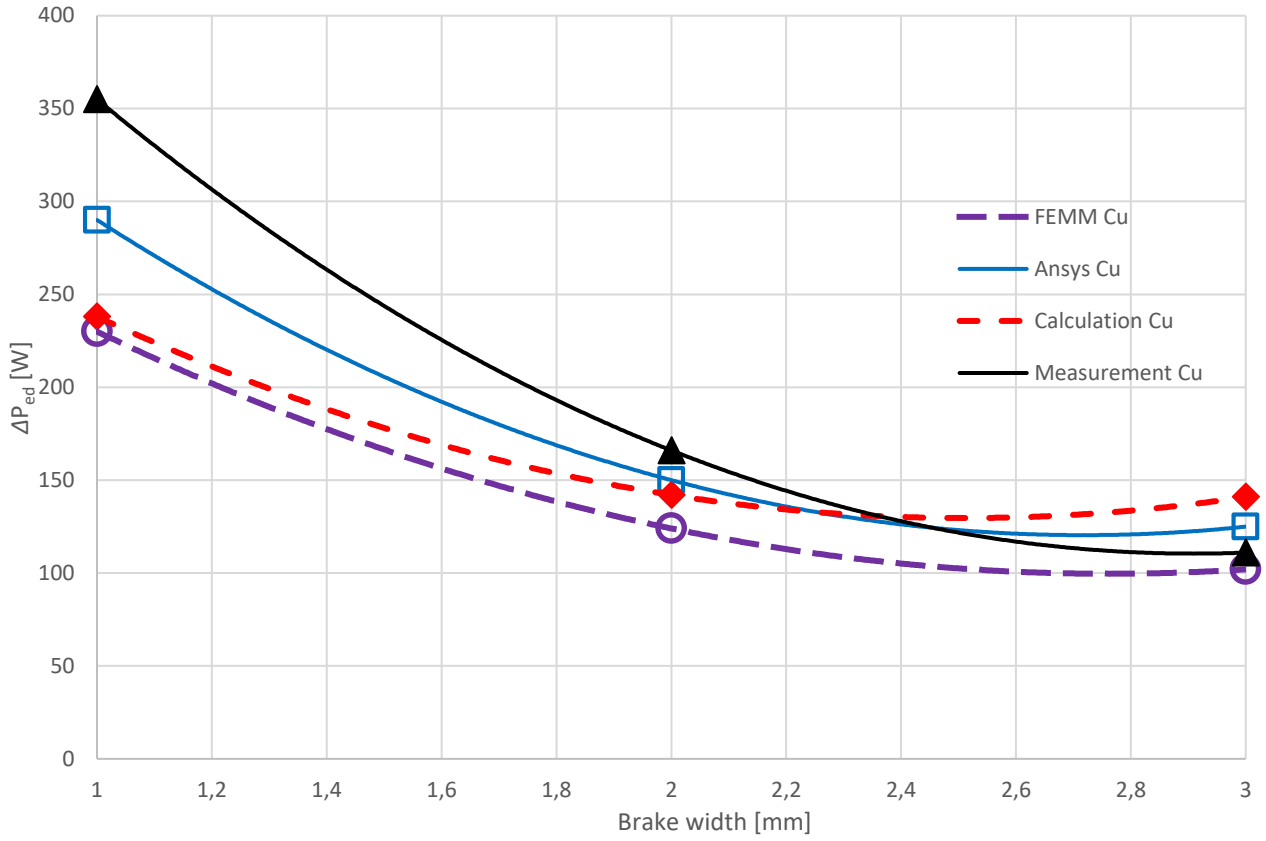

Fig 8.3 Braking power in copper ECB versus width of conductor at 100 krpm

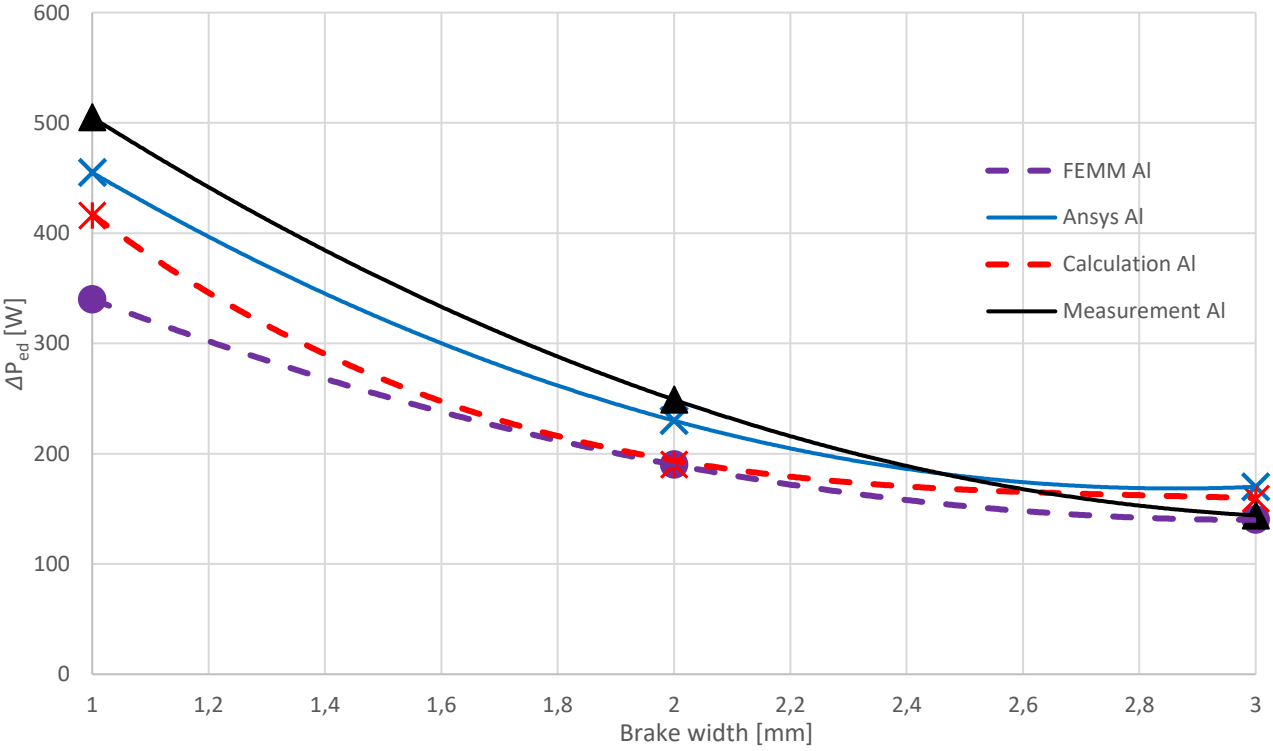

Fig 8.4 Braking power in aluminum ECB versus width of conductor at 100 krpm

8.3 Results for 150 krpm

150 krpm	brake width	B_{yCM}	FEMM	Ansys	Calculation	Measurement
			ΔP_{ed_FEMM}	ΔP_{ed_Ansys}	ΔP_{ed_cal}	ΔP_{ed_meas}
	[mm]	[T]	[W]	[W]	[W]	[W]
Cu	3	0,046	130	160	214	150
Cu	2	0,0455	140	170	199	201
Cu	1	0,056	240	300	239	363
Al	3	0,055	164	200	226	218
Al	2	0,057	206	250	223	305
Al	1	0,092	380	470	390	543

Table 8.3 Comparison of measured losses in ECB at speed 150 krpm with simulations in FEMM and Ansys Maxwell 2D and analytical calculation

In Table 8.3 are shown results of simulations, calculation and measurement for 150 krpm. Fig 8.5 and Fig 8.6 shows dependency of braking power on brake conductor width. With higher frequency (rotation speed) is the value of skin depth lower. For both materials it is 2 mm or lower, that yield in almost stable value of magnetic flux density beyond this depth. For this reason are analytical calculation and simulations value of braking power almost the same for 2 and 3 mm brake width.

It turned out that the ECB losses for 150 krpm are sufficient to measure the torque.

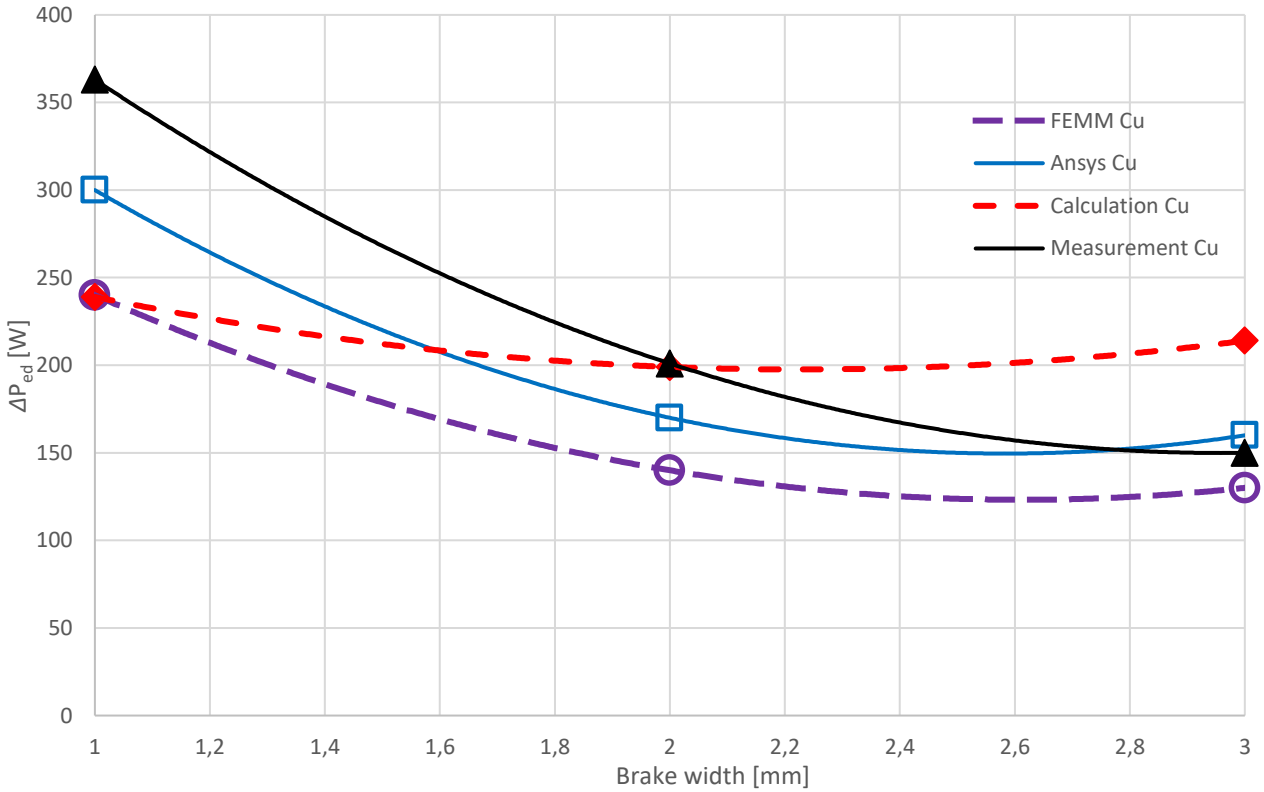

Fig 8.5 Braking power in copper ECB versus width of conductor at 150 krpm

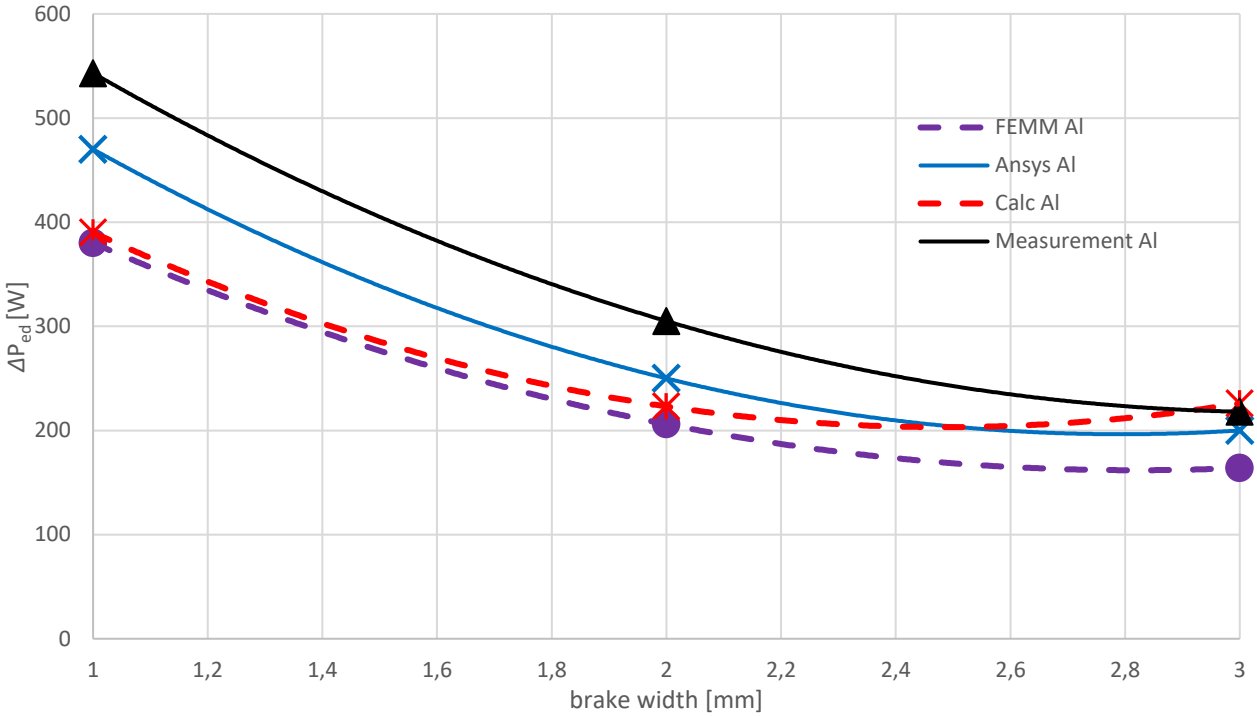

Fig 8.6 Braking power in aluminum ECB versus width of conductor at 150 krpm

8.4 Results for 200 krpm

200 krpm	brake width	B_{yCM}	FEMM	Ansys	Calculation	Measurement
			ΔP_{ed_FEMM}	ΔP_{ed_Ansys}	ΔP_{ed_cal}	ΔP_{ed_meas}
	[mm]	[T]	[W]	[W]	[W]	[W]
Cu	3	0,041	160	195	266	224
Cu	2	0,041	154	190	256	276
Cu	1	0,044	246	300	242	391
Al	3	0,049	190	235	281	278
Al	2	0,05	220	260	274	354
Al	1	0,068	394	475	390	564

Table 8.4 Comparison of measured losses in ECB at speed 200 krpm with simulations in FEMM and Ansys Maxwell 2D and analytical calculation

In Table 8.4 are shown results of simulations, calculation and measurement for 200 krpm. Fig 8.7 and Fig 8.8 shows dependency of braking power on brake conductor width. As can be seen in equation (5.33) losses are only exponentially rising. In fact, however, with increasing brake width and frequency, they fall. It is caused by reactance, which is not included into analytical calculation equations. For this reason is Eddy current loss from analytical calculation in Fig 8.7 and Fig 8.8 rising. The inaccuracy of the analytical calculation is also based on the fact that only

the fundamental is considered. Obviously simulations are more accurate due to considering the whole spectrum.

It turned out that the ECB losses for 200 krpm are insufficient to measure the torque.

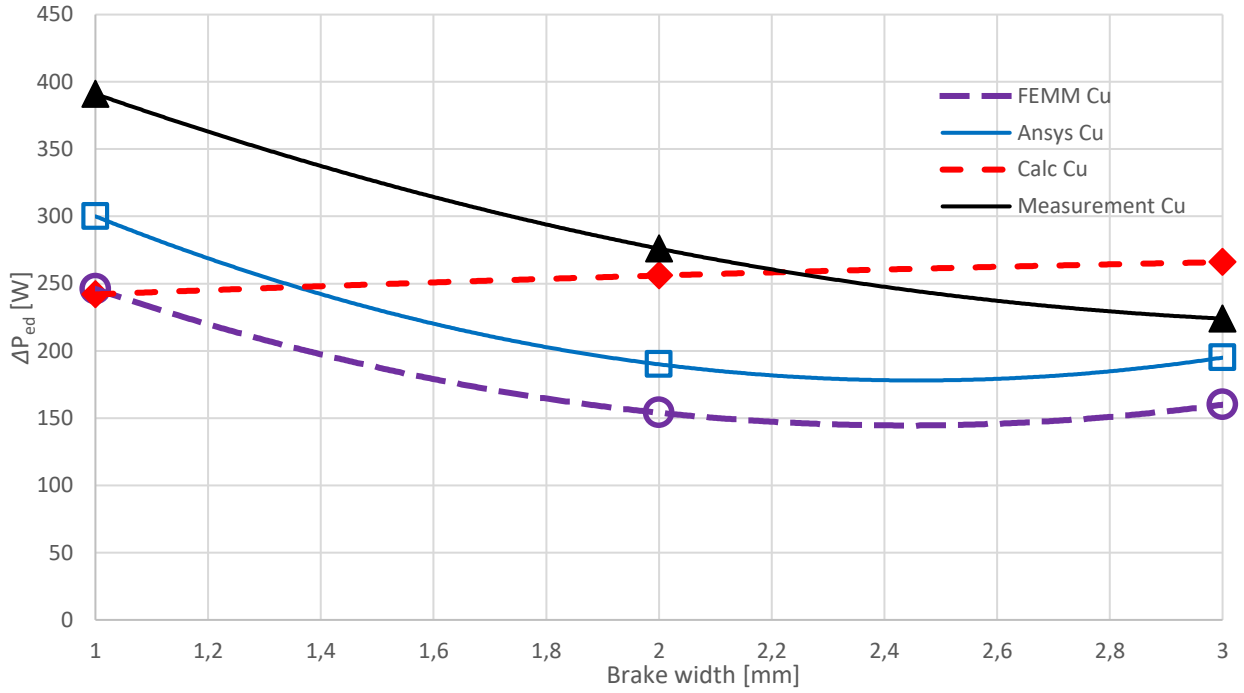

Fig 8.7 Braking power in copper ECB versus width of conductor at 200 krpm

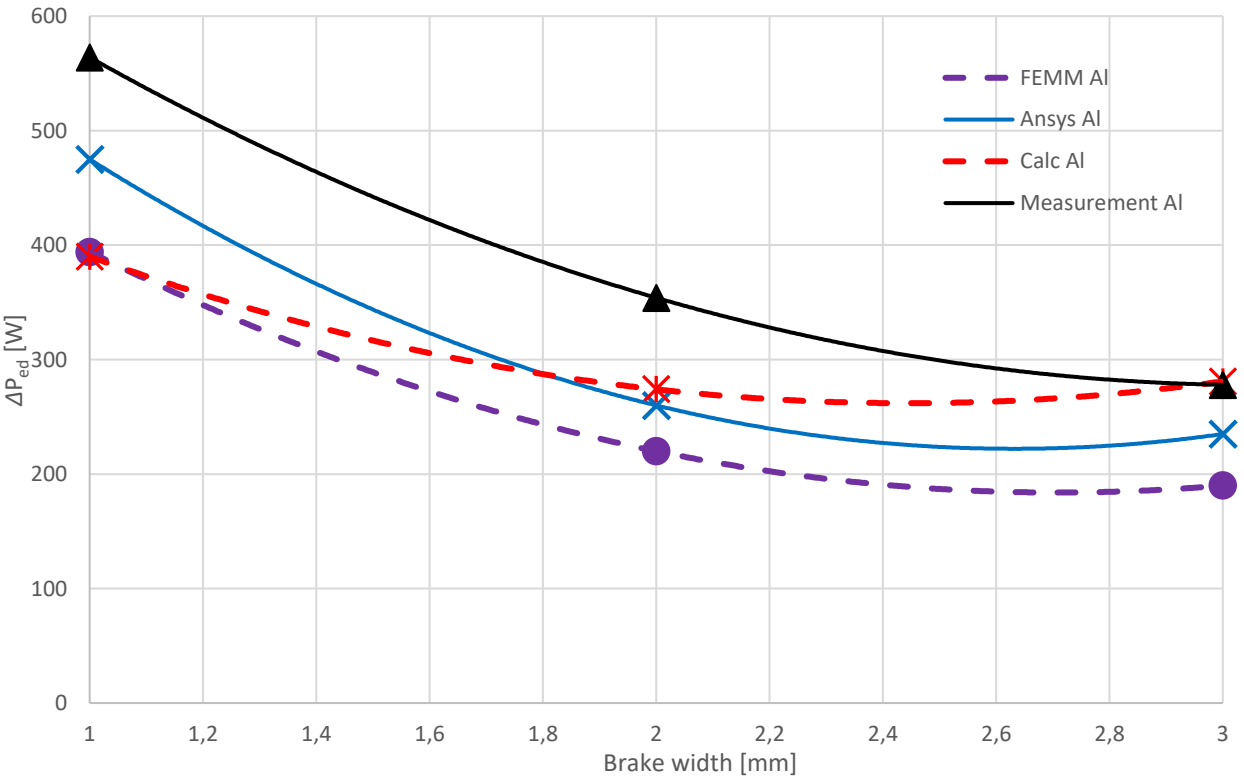

Fig 8.8 Braking power in aluminum ECB versus width of conductor at 200 krpm

CONCLUSION

The work is focused on the measurement of very high speed machines, which are in recent trend, for their compact size and low weight. The problem occurs when the torque is measured above 50 krpm. The thesis is therefore aimed at finding a torque measurement method above these speeds.

In the beginning of thesis is described slotless VHS, which is going to be measured. Several methods of VHS torque measurement are presented and one of them, Eddy current brake method, is chosen. In chapter 4. is described principle of Eddy current brake and its types. Chapter 5. deals with analytical calculation of Eddy currents, which helps us to understand deeper the physical phenomena.

To verify the results of the analytical calculation, a 2D model of the given brake was created in the program FEMM and Ansys/Maxwell. Using the Finite Element Method, two main conductors were examined: Copper and Aluminum, with varying brake widths of the conductive drum and with back iron placed behind the brake conductor for speeds ranging from 50 to 200 krpm.

Prototypes of ECB were made, according to initial simulations and materials in stock, in the beginning of the thesis. These prototypes were measured and examined whether their braking power is sufficient for torque measurement. Measured data were used to verify the results from the calculation and simulations. It can be said that measured and calculated data show a good match for lower speed (till 100 krpm) despite a number of simplifications. Above this speed are curves already different, especially due to the absence of influence of the reactance in the calculation, which would reduce the value of the losses in the brake with a greater width, and absence of the whole spectrum of higher harmonics in the calculation.

It turned out that ECB losses for 200 krpm are insufficient for proper measurement of torque. Sufficient value of braking power could be achieved by extending the permanent magnet length with respect to the rotor dynamics and by lowering conductivity of conductive drum in ECB. It would be worth to consider using magnets with higher thermal resistance, since the temperatures in ECB are quite high.

Literature

[1] Analytical and Experimental Investigation of a Low Torque, Ultra-High Speed Drive System. ZWYSSIG, C., S. D. ROUND a J. W. KOLAR. Conference Record of the 2006 IEEE Industry Applications Conference Forty-First IAS Annual Meeting. 2006. ISBN 1-4244-0364-2.

[2] N. Bianchi, S. Bolognani, and F. Luise, "Potentials and limits of highspeed PM motors," IEEE Transactions on Industry Applications, vol. 40, no. 6, pp. 1570–1578, 2004.

[3] LIPING, Zheng. SUPER HIGH-SPEED MINIATURIZED PERMANENT MAGNET SYNCHRONOUS MOTOR [online]. 2005 [cit. 2018-01-03]. University of Central Florida.

[4] Very High Speed Slotless Permanent Magnet Motors: Analytical Modeling, Optimization, Design and Torque Measurement Methods. PFISTER, P.-D. a Y. PERRIARD. IEEE Transactions on Industrial Electronics. 2009, 296 - 303. ISBN 0278-0046.

[5] Torque measurement methods for very high speed synchronous motors. PFISTER, P.-D. a Y. PERRIARD. 2008 18th International Conference on Electrical Machines. IEEE, 2008. ISBN 978-1-4244-1735-3.

[6] SOKOLOV, Georgii. Analysis of electrodynamic brake for utilization in systems with rotating shafts [online]. 2016 [cit. 2018-01-03]. Saimaa University of Applied Sciences.

[7] KUREK, Michal. Modernizácia riadenia vírivej brzdy [online]. 2008 [cit. 2018-01-03]. ŽILINSKÁ UNIVERZITA V ŽILINE.

[8] Design and Finite Element Analysis of a Radial-Flux Salient-Pole Eddy Current Brake. SINMAZ, Ali, Mehmet Onur GULBAHCE a Derya Ahmet KOCABAS. 2015 9th International Conference on Electrical and Electronics Engineering (ELECO). IEEE, 2015. ISBN 978-6-0501-0737-1.

[9] Vítek, O. Vysokootáčkové elektrické motory, Brno: Vysoké učení technické v Brně, Fakulta elektrotechniky a komunikačních technologií, 2016. 114 s. Habilitační práce.

[10] HELLER, Bedřich a HAMATA, Václav. Přídavná pole, síly a ztráty v asynchronním stroji. 1. vyd. Praha: Československá akademie věd, 1961, 202 s.

[11] MEEKER, David. Analysis of an Eddy Current Brake with FEMM [online]. [cit. 2018-05-14]. Dostupné z: http://www.femm.info/wiki/Examples

List of symbols, quantities and abbreviations

BI	back iron
ECB	eddy current brake
FEM	Finite element method
FEMM	Finite element method magnetic
krpm	kilo revolutions per minute
PMSM	Permanent magnet synchronous motor
VHS	very high speed
A	area [m^2]
Al	aluminum
B	magnetic flux density [T]
B_y	component of magnetic flux density in direction of y axis [T]
B_{y0m}	amplitude of magnetic flux density in y axis direction [T]
Cu	copper
D_c	diameter of conductor drum [m]
D_{Fe}	inner diameter if back iron [m]
E	electric field intensity [$V \cdot m^{-1}$]
$EMF\ (\varepsilon)$	electromotive force [V]
h	brake width [m]
H	intensity of magnetic field [$A \cdot m^{-1}$]
H_0	amplitude of intensity of magnetic field [$A \cdot m^{-1}$]
H_x, H_y	components of magnetic field intensity in direction of axis x and y [$A \cdot m^{-1}$]
I	Inertia [$kg \cdot m^2$]
I_{ed}	Eddy current [A]
J	current density [$MA \cdot m^{-2}$]
J_z	component of current density in direction of z axis [$MA \cdot m^{-2}$]
l_c	height of conductor [m]
l_{PM}	length of permanent magnet [m]
ΔP_{ed}	Eddy current loss [W]
Δp_{ed}	Eddy current loss per unit of area [$W \cdot m^{-2}$]
R	resistance [Ω]
T	Torque [Nm]
t	time [s]
v	velocity [m·s]
β_k	complex coefficient in Eddy current calculation [-]
β_{ka}, β_{kb}	real and imaginary components of β_k
Φ	magnetic flux [Wb]
δ	Skin depth [m]

σ	electrical conductivity of material [MS·m^{-1}]
μ_r	relative permeability [-]
μ_0	permeability of vacuum [H·m^{-1}]
ω	angular velocity [rad^{-1}]
ρ	electrical resistivity [Ω·m]
τ_p	pole pitch [m]
ϑ	temperature [°C]